Analytic First-Order Derivatives of CASPT2 Combined with the Polarizable Continuum Model

Yoshio Nishimoto*

Graduate School of Science, Kyoto University, Kyoto 606-8502, Japan

E-mail: nishimoto@kuchem.kyoto-u.acjp

December 29, 2024

Abstract

The complete active space second-order perturbation theory (CASPT2) is valuable for accurately predicting electronic structures and transition energies. However, optimizing molecular geometries in the solution phase has proven challenging. In this study, we develop analytic first-order derivatives of CASPT2 using an implicit solvation model, specifically the polarizable continuum model (PCM), within the open-source package OpenMolcas. Analytic gradients and non-adiabatic coupling vectors are computed by solving a modified Z-vector equation. Comparisons with existing theoretical and experimental results demonstrate that the solvent effects can be qualitatively captured using the developed method.

1

1 Introduction

The electron correlation is formally divided into the "static" and "dynamical" electron correlations, both of which must be considered for accurate quantum chemical calculations. The former is typically described by the multiconfiguration self-consistent field (MCSCF) method, where the wavefunction is expressed as a linear combination of selected configuration state functions (CSFs). A particularly useful variant of the MCSCF method is the complete active space SCF (CASSCF) method. In this approach, an active space is defined, and the wavefunction is obtained by performing full configuration interaction (CI) within this active space. The latter, dynamical or non-static electron correlation, is generally treated with post-MCSCF methods, commonly referred to as multireference (MR) methods, such as MR coupled-cluster (MRCC)[1–3] and configuration interaction (MRCI).[4] Although these two MR approaches are highly accurate, their computational cost is significant. Another class of MR approaches is perturbation theory (MRPT), with the complete active space second-order perturbation theory (CASPT2)[5–7] being one of the most well-known MRPTs. Note that the "static" electron correlation computed with the MCSCF method can contain contributions that should belong to the dynamical electron correlation in modern electron correlation theory.[8,9] They are referred to as the "internal" dynamical electron correlation, and the rest, taken account by post-MCSCF methods, is referred to as the "external" dynamical correlation. These post-SCF treatments can also be applied to the single-configuration Hartree–Fock method. In particular, the CC approach can be extended to excited states through the equation-of-motion (EOM) formalism,[10] typically utilizing the CC singles and doubles (EOM-CCSD) method.

Since many chemical events occur in solution, it is highly desirable to include solvent effects in the aforementioned accurate quantum chemical calculations. A straightforward approach is to treat solvent molecules explicitly; however, the number of atoms to consider in this manner can be substantial. Even with advancements in the quantum mechanical/molecular mechanical (QM/MM) method,[11] the computational cost of such calculations remains relatively high. One challenge in achieving accurate QM/MM calculations arises from the sampling required to ensure convergence of the free energy, which may be addressed using a reweighting technique.[12] Another class of

2

explicit solvent models includes the effective fragment potential,[13,14] enabling a more accurate treatment of solvent molecules. On the other hand, solvent effects can also be efficiently considered in an implicit manner. This class includes the generalized Born model,[15,16] the polarizable continuum model (PCM),[17] the conductor-like screening model (COSMO),[18] and the reference interaction site model (RISM).[19,20] The first three approaches are known as the dielectric model and have a relatively modest computational demand compared to that of RISM. Among these methods, the PCM approach is widely utilized and has been combined with various computational methodologies. These primarily include single-configuration methods, though some earlier studies have incorporated electron correlation methods.[21–24]

Determining molecular structures using a combination of accurate quantum chemical methods and implicit solvent models, particularly for excited states, remains challenging. One difficulty is developing the analytic derivative with respect to the atomic coordinates. A notable example is the combination of EOM-CCSD or symmetry-adapted cluster-configuration interaction (SAC-CI) with PCM, as demonstrated by Cammi,[25,26] which has been applied to absorption and emission energies. The integration with multiconfiguration methods is less common, though some earlier studies exist.[20,27–30] However, the integration with MRPT is much more limited. Noteworthy developments by Yamazaki[31] (with CASSCF) and Mori[32] employed the RISM method to incorporate non-equilibrium solvent effects and applied it to finding conical intersections (CoIns). Unfortunately, the program code for these methods is not publicly available. Additionally, some studies have successfully incorporated explicit solvents (QM/MM) at the MRPT level,[33,34] which is useful for including kinetic effects. Technically, the electronic coupling between solute and solvent molecules is typically decoupled in QM/MM calculations, allowing for the use of program code developed for vacuum with minimal modifications. While this approach can be beneficial in many situations, the standard (non-polarizable) QM/MM method employs a fixed charge in the MM region, which is unsuitable when the electronic structure of the solvent varies following an electronic transition. In contrast, implicit solvation models account for a solvent charge dependency on the solute's electronic structure, necessitating additional development for analytic derivatives

3

with PCM and possibly for polarizable QM/MM methods.[35]

In this study, we develop analytic first-order derivatives (gradients and non-adiabatic coupling vectors) for the state-averaged (SA) MCSCF and CASPT2 methods in combination with the conductor PCM (C-PCM) within the open-source package OpenMolcas.[36–38] The CASPT2 energy is obtained using the perturbation to energy (PTE) approach,[39] where the solvent reaction field is generated at the SCF level and remains fixed during the PT2 calculation. While it is theoretically possible to generate the reaction field at the CASPT2 level by iteratively determining the solvent charge and solute density (perturbation to energy and density; PTED), this approach appears impractical for applications and thus is not considered here. This study primarily focuses on the CASSCF-based wavefunction, but the developed method can also be applied to the restricted active space (RAS)[40] SCF and the PT2 extension (RASPT2).[41,42] The developed method is applied to typical molecules, focusing on solvent effects.

2   Methodology

In this section, the following indices are used without further notation:

- General molecular orbitals (MOs): p, q, r, s, t, u

- Internal states: $\alpha, \beta, \gamma, \eta, \theta \ (\in \mathscr{P})$

- General states: $\pi, \rho \ (\in \mathscr{P} + \mathscr{P}^{\perp})$

- Tesserae: i, j

$\mathscr{P}$ denotes the reference space, which typically includes the states averaged in the reference SCF calculation. It is assumed that all states are equally averaged in SCF and included in the PT2 calculation. Conversely, $\mathscr{P}^{\perp}$ represents the orthogonal complement to $\mathscr{P}$. States within $\mathscr{P}$ and $\mathscr{P}^{\perp}$ are commonly referred to as internal and external states, respectively.

4

2.1 PCM for Single-Configuration Methods

In PCM, the solute–solvent interface is defined using discretized surface elements known as tesserae. Each tessera carries a polarizable charge called the apparent surface charge (ASC) Q_i, which is used to evaluate the electrostatic interaction between the solute and solvent. The ASCs are determined by solving a matrix equation, the specifics of which depend on the chosen PCM model. For the C-PCM used in this study, the equation is given by:

$$\mathbf{Q} = -\frac{\varepsilon - 1}{\varepsilon}\mathbf{C}^{-1}\mathbf{V} \tag{1}$$

with

$$\begin{cases} C_{i,i} & = 1.0694\sqrt{\frac{4\pi}{a_i}} \\ C_{i,j} & = \frac{1}{|\mathbf{r}_i - \mathbf{r}_j|} \end{cases}, \tag{2}$$

where a_i and $\mathbf{r}_i$ represent the area and center of tessera i, respectively, and ε is the dielectric constant (relative permittivity) of the solvent. $\mathbf{V}$ is the sum of the nuclear and electronic electrostatic potentials (ESP) of the solute: $\mathbf{V} = \mathbf{V}^{\mathrm{N}} + \mathbf{V}^{\mathrm{e}}$ with

$$V_i^{\mathrm{N}} = \sum_{\zeta} \frac{Z_\zeta}{|\mathbf{r}_\zeta - \mathbf{r}_i|} \tag{3}$$

$$V_i^{\mathrm{e}} = -\sum_{p,q} D_{p,q} \left\langle p \left| \frac{1}{|\mathbf{r} - \mathbf{r}_i|} \right| q \right\rangle , \tag{4}$$

where Z_ζ and $\mathbf{r}_\zeta$ are the nuclear charge and coordinates of atom ζ, $\mathbf{r}$ is the electronic coordinate, and $D_{p,q}$ is the solute's density matrix. Thus, ASCs can be calculated separately by solving Eq. (1): $\mathbf{Q} = \mathbf{Q}^{\mathrm{N}} + \mathbf{Q}^{\mathrm{e}}$. Since $\mathbf{V}^{\mathrm{e}}$ and, consequently, $\mathbf{Q}^{\mathrm{e}}$ depend on the solute density, the electrostatic contribution to the (one-electron) Hamiltonian is updated at each SCF cycle.

The free energy of the solute–solvent system is typically expressed as:

$$\mathscr{G} = E^{\mathrm{solute}} + \frac{1}{2}E^{\mathrm{int}} + \mathscr{G}^{\mathrm{non\text{-}es}}, \tag{5}$$

5

where E^{solute} is the solute's internal energy, E^{int} is the electrostatic interaction energy between the solute and solvent, and $\mathscr{G}^{\text{non-es}}$ is the sum of the non-electrostatic cavitation, dispersion, and repulsion free energies. E^{int} is generally given by:

$$E^{\text{int}} = \sum_i V_i Q_i \ . \tag{6}$$

While E^{solute} is computed as in vacuum, the wavefunction parameters are determined in the presence of the solvent's reaction field. Half of E^{int} accounts for the work required to polarize the dielectric medium when a polarized solute molecule is inserted into the cavity, making the total energy a free energy. Thus, the free energy is obtained with consistent densities for both the solute and solvent.

If the solute wavefunction is written as Ψ, the solute–solvent free energy can be explicitly written as:

$$\begin{aligned}
\mathscr{G} &= \left\langle \Psi \middle| \hat{H}^{\text{vac}} \middle| \Psi \right\rangle + \frac{1}{2} \sum_i V_i Q_i + E_{\text{nuc}} + \mathscr{G}^{\text{non-es}} \\
&= \left\langle \Psi \middle| \hat{H}^{\text{vac}} + \hat{V} \middle| \Psi \right\rangle - \frac{1}{2} \sum_i V_i^{\text{e}} Q_i^{\text{e}} + \frac{1}{2} \sum_i V_i^{\text{N}} Q_i^{\text{N}} + E_{\text{nuc}} + \mathscr{G}^{\text{non-es}}.
\end{aligned} \tag{7}$$

Here, $\hat{H}^{\text{vac}}$ is the vacuum Hamiltonian, $\hat{V}$ is the electrostatic operator from the solvent, and E_{nuc} is the nuclear repulsion energy of the solute molecule. The wavefunction Ψ is obtained by minimizing the free energy (Eq. (7)) with respect to wavefunction parameters, and the electrostatic operator $\hat{V}$ is

$$\hat{V} = \sum_{p,q} \hat{E}_{p,q} \mathscr{V}_{p,q} = - \sum_{p,q} \hat{E}_{p,q} \sum_i \left\langle p \middle| \frac{Q_i}{|\mathbf{r} - \mathbf{r}_i|} \middle| q \right\rangle . \tag{8}$$

In Eq. (7), the second term subtracts the double counting of electron–electron interactions from the first term, while the third term accounts for the electrostatic interaction between the solute nuclei and the ASCs induced by the solute nuclei. If only one state is involved in the computation, the definition of free energy and the computation process is straightforward. In this study, we do not consider $\mathscr{G}^{\text{non-es}}$ further in the derivation and computation.

6

2.2 SA-MCSCF/PCM

Unlike single-state methods, the free energy for multistate methods cannot be uniquely defined. The most physically and mathematically rigorous approach is to use the state-specific or single-state MCSCF (SS-MCSCF) energy and density, allowing the free energy of the solute–solvent system to be defined similarly to the single-state case (Eq. (7)). However, it is well known that SS-MCSCF calculations for excited states suffer from the root-flipping problem,[43] making them impractical for many applications. For locating minimum energy CoIn (MECoIn), it is usually necessary that the two (or more) crossing states are orthogonal, which SS-MCSCF calculations cannot easily satisfy. Furthermore, using a single reference state may be insufficient for MRPT calculations, where multistate or quasi-degenerate MRPT methods are often required to achieve satisfactory accuracy. Therefore, a widely accepted approach for accurate quantum chemical calculations in vacuum is to average over several states during the MCSCF calculation, followed by MRPT calculations if possible. Although pursuing the SS-MCSCF approach is an interesting avenue of research,[44] the prevailing method for excited-state calculations with multiconfigurational approaches is to SA-MCSCF.

However, combining SA-MCSCF with PCM is not straightforward. Ideally, we would want the solute energy to be state-averaged (equally, in most cases) while the solvent is polarized by the state-specific density, and the state-averaged energy can be variationally optimized. Unfortunately, formulations that satisfy these requirements do not appear to be available. If we assume that both the solute energy and solvation density are averaged in the same manner, it is possible to variationally minimize the state-averaged energy. However, it is difficult to imagine a scenario where the solvent is naturally polarized by the equally averaged density, making this situation unrealistic. In earlier work by Song,[27] the state-averaged energy is obtained using fixed or dynamic weights, leading to (quasi-)state-specific and state-averaged characteristics around the minimum energy and CoIn regions, respectively. The dynamically weighted solvation scheme[35] is particularly useful for molecular dynamics simulations. However, in electron transitions, the transition probability strongly depends on the character of the excitation (i.e., whether it is allowed or forbidden), so a

state-specific solvation model is ultimately needed. On the other hand, using different densities for solute and solvent polarization complicates the variational minimization process, as discussed below. Additionally, this approach introduces another type of root-flipping problem when selecting the density for polarizing the solvent.[35]

Since it is not possible to formulate a physically and mathematically satisfying model in a straightforward manner, the original formulation implemented in OpenMolcas is used in this study. One of the earliest PCM calculations with (Open)Molcas can be traced back to the work in Refs. 45–47, and there are several studies[48–52] that employ SA-CASSCF or CASPT2 calculations with PCM as implemented in (Open)Molcas. Despite the challenges outlined here, SA-MCSCF and CASPT2 calculations with PCM remain valuable methods.

2.2.1 SA-MCSCF/PCM energy

In vacuum, the SA-MCSCF calculation averages adiabatic energies as follows:

$$E_{\text{ave}} = \sum_{\gamma \in \mathscr{P}} \omega_\gamma \left\langle \Psi_\gamma^{(0)} \left| \hat{H}^{\text{vac}} \right| \Psi_\gamma^{(0)} \right\rangle + E_{\text{nuc}} \tag{9}$$

where ω_γ is the weight for state-averaging, which in many cases is the inverse of the number of internal states, and satisfies the normalization condition: $\sum_{\gamma \in \mathscr{P}} \omega_\gamma = 1$. The zeroth-order wave-function $\Psi_\gamma^{(0)}$ is expressed as a linear combination of CSFs Φ_I

$$\Psi_\gamma^{(0)} = \sum_I c_{I,\gamma} \Phi_I \,, \tag{10}$$

where $c_{I,\gamma}$ is the expansion (CI) coefficients.

Based on the equally state-averaged MCSCF energy, we aim to optimize molecular geometries at the state ϕ ($\in \mathscr{P}$) with which the solvent charges are polarized. Under this assumption, we first

8

define the free energy of the state ϕ, analogously to the single-state case (Eq. (7)):

$$\mathscr{G}_\phi^{[\phi]} = \left\langle \Psi_\phi^{(0)} \left| \hat{H}^{\text{vac}} \right| \Psi_\phi^{(0)} \right\rangle + \frac{1}{2} \sum_i V_i^{[\phi]} Q_i^{[\phi]} + E_{\text{nuc}}$$

$$= \left\langle \Psi_\phi^{(0)} \left| \hat{H}^{\text{vac}} + \hat{V}^{[\phi]} \right| \Psi_\phi^{(0)} \right\rangle - \frac{1}{2} \sum_i V_i^{\text{e},[\phi]} Q_i^{\text{e},[\phi]} + \frac{1}{2} \sum_i V_i^{\text{N}} Q_i^{\text{N}} + E_{\text{nuc}} . \tag{11}$$

Here, "$[\phi]$" denotes the state used to generate the reaction field. The electrostatic operator $\hat{V}^{[\phi]}$ can be written as:

$$\hat{V}^{[\phi]} = \sum_{p,q} \hat{E}_{p,q} \mathscr{V}_{p,q}^{[\phi]} = \frac{\varepsilon - 1}{\varepsilon} \sum_{i,j} \sum_{p,q} \hat{E}_{p,q} \left\langle p \left| \frac{1}{|\mathbf{r} - \mathbf{r}_i|} \right| q \right\rangle \left(\mathbf{C}^{-1} \right)_{i,j} V_j^{[\phi]} \tag{12}$$

Hereafter, the superscript on the integral $\mathscr{V}_{p,q}^{[\phi]}$ refers to the density used to polarize the ASC:

$$\mathscr{V}_{p,q}^{\text{A}} := \mathscr{V}_{p,q}(\mathbf{D}^{\text{A}})$$

$$= -\frac{\varepsilon - 1}{\varepsilon} \sum_{i,j} \left\langle p \left| \frac{1}{|\mathbf{r} - \mathbf{r}_i|} \right| q \right\rangle \left(\mathbf{C}^{-1} \right)_{i,j} \sum_{r,s} \left\langle r \left| \frac{1}{|\mathbf{r} - \mathbf{r}_j|} \right| s \right\rangle D_{r,s}^{\text{A}} \tag{13}$$

Similarly, the energy for state $\gamma \in \mathscr{P}$ is written as:

$$\mathscr{E}_\gamma^{[\phi]} = \left\langle \Psi_\gamma^{(0)} \left| \hat{H}^{\text{vac}} + \hat{V}^{[\phi]} \right| \Psi_\gamma^{(0)} \right\rangle - \frac{1}{2} \sum_i V_i^{\text{e},[\phi]} Q_i^{\text{e},[\phi]} + \frac{1}{2} \sum_i V_i^{\text{N}} Q_i^{\text{N}} + E_{\text{nuc}} \tag{14}$$

If $\gamma = \phi$, Eq. (14) becomes identical to Eq. (11), which represents the free energy. Since the primary focus of this study is to optimize molecular geometries for a specific state, the energy for $\gamma = \phi$ is the most important energy to define rigorously. On the other hand, the energy of other states ($\gamma \neq \phi$) does not have a simple form and lacks straightforward physical interpretation. Therefore, transition energies should be evaluated as differences between two separate calculations. Finally,

9

the state-averaged energy can be expressed as:

$$\mathscr{E}_{\text{SA}}^{[\phi]} = \omega_\phi \mathscr{G}_\phi^{[\phi]} + \sum_{\gamma \neq \phi \in \mathscr{P}} \omega_\gamma \mathscr{E}_\gamma^{[\phi]}$$

$$= \sum_{\gamma \in \mathscr{P}} \omega_\gamma \left\langle \Psi_\gamma^{(0)} \left| \hat{H}^{\text{vac}} + \hat{V}^{[\phi]} \right| \Psi_\gamma^{(0)} \right\rangle - \frac{1}{2} \sum_i V_i^{\text{e},[\phi]} Q_i^{\text{e},[\phi]} + \frac{1}{2} \sum_i V_i^{\text{N}} Q_i^{\text{N}} + E_{\text{nuc}} \qquad (15)$$

This expression has been used in (Open)Molcas.

One drawback of the above formulation is that the current implementation does not yield a correct variational energy. This is because the electronic gradient and Hessian used during SCF calculations is approximated such that the algorithm remains consistent with that of the gas phase calculation. The approximation introduced in the electronic gradient assumes that the state-averaged and state-specific ASCs are identical, as described in the Appendix (Eqs. (50) and (51)), and the approximate orbital Hessian should be the first term in Eq. (52). While this is clearly not the case and remains a crude approximation, we expect that solutions obtained using approximate gradients and Hessian will still be reasonably close to the true solution, provided iterative optimization converges.[53] With PCM, SCF convergence is indeed slower and may suffer from another type of root-flipping problem, particularly for excited states.

2.2.2 SA-MCSCF/PCM gradients

We now consider the analytic differentiation of the energy $\mathscr{E}_\gamma^{[\phi]}$. Once SCF convergence is achieved, the conventional SA-MCSCF energy (in the gas phase) remains invariant with respect to internal and external state rotations. However, when applying the formulation from the previous section, this invariance does not hold for states $\gamma \neq \phi$. Moreover, due to the unequal averaging of the solute density for polarizing the ASCs, the SA-MCSCF energy is not invariant under rotations between internal states. While the following formulation and implementation are valid for $\gamma \neq \phi$, in this study, we restrict calculations to cases where $\gamma = \phi$, as the energy for $\gamma \neq \phi$ lacks physical significance.

Although the state-averaged energy is not variationally minimized, this does not preclude the

10

formulation of analytic derivatives. We only need the conditions that are satisfied at the convergence of SCF. With this in mind, the Lagrangian used in this study is as follows:

$$
\begin{aligned}
\mathscr{L}_{\gamma}^{[\phi]} &= \mathscr{E}_{\gamma}^{[\phi]} + \mathscr{L}_{\gamma}^{\mathrm{SCF},[\phi]} \\
&= \mathscr{E}_{\gamma}^{[\phi]} + \sum_{p,q} \overline{\kappa}_{p,q}^{\gamma,[\phi]} \frac{\partial \widetilde{\mathscr{E}}_{\mathrm{SA}}^{[\phi]}}{\partial \kappa_{p,q}} + \sum_{\eta \in \mathscr{P}} \sum_{\pi > \eta} \overline{P}_{\eta,\pi}^{\gamma,[\phi]} \frac{\partial \widetilde{\mathscr{E}}_{\mathrm{SA}}^{[\phi]}}{\partial P_{\eta,\pi}}
\end{aligned}
\tag{16}
$$

The first term is the energy of the target state γ to be differentiated (free energy if $\gamma = \phi$). In vacuum, the second term represents the generalized Brillouin condition, and the third term is the CI condition. The last two terms ($\mathscr{L}_{\gamma}^{\mathrm{SCF},[\phi]}$) are constraint conditions that are themselves equal to zero. The explicit form of these partial derivatives is provided in the Appendix (Eqs. (50) and (51)). In the conventional SA-MCSCF, these terms relate to the partial derivatives of the SA-MCSCF energy. The coefficients $\overline{\kappa}_{p,q}^{\gamma,[\phi]}$ and $\overline{P}_{\eta,\pi}^{\gamma,[\phi]}$ are the multipliers to be determined.

Next, we derive the Z-vector equation to be solved:

$$
\frac{\partial \mathscr{L}_{\gamma}^{[\phi]}}{\partial \kappa_{r,s}} = \frac{\partial \mathscr{L}_{\gamma}^{[\phi]}}{\partial P_{\theta,\rho}} = 0
\tag{17}
$$

for all independent rotations of r, s and θ, ρ. This results in the following linear matrix equation:

$$
\mathbf{A} \begin{pmatrix} \overline{\boldsymbol{\kappa}}^{\gamma,[\phi]} \\ \overline{\mathbf{P}}^{\gamma,[\phi]} \end{pmatrix} = - \begin{pmatrix} (\partial \mathscr{E}_{\gamma}^{[\phi]})/(\partial \boldsymbol{\kappa}) \\ (\partial \mathscr{E}_{\gamma}^{[\phi]})/(\partial \mathbf{P}) \end{pmatrix}
\tag{18}
$$

The explicit expressions of the approximate Hessian $\mathbf{A}$ are given in Appendix [Eqs. (52), (54), (55), and (57)]) The right-hand side is obtained by taking the partial derivative of the energy $\mathscr{E}_{\gamma}^{[\phi]}$. Unlike the conventional SA-MCSCF, the partial derivative with respect to CI coefficients (state transfer parameters) is not necessarily zero when $\gamma \neq \phi$. While the formulation here includes only orbital and CI rotation parameters, it is also possible to treat the ASC as wavefunction parameters in an equivalent fashion.[27] However, since ASCs depend on relatively simple functions (for C-PCM), they need not be treated explicitly as parameters.

11

Because the constraint conditions above do not correspond to the first-order derivatives of $\mathscr{E}_{\text{SA}}^{[\phi]}$ with respect to wavefunction parameters, the expressions in Eqs. (52)–(57) are not exact second-order derivatives of $\mathscr{E}_{\text{SA}}^{[\phi]}$. They are approximate Hessians and, more precisely, are exact first-order derivatives of the approximate electronic gradient. The matrix $\mathbf{A}$ is no longer symmetric (and maybe non-positive definite), so the conventional preconditioned conjugate gradients method cannot be used for improved convergence. In this study, the conjugate gradients squared (CGS) method[54,55] is employed. Preconditioning is also implemented according to Algorithm 4 in Ref. 55. Using CGS, the linear equation can be solved without explicitly considering the transpose of matrix $\mathbf{A}$, and there is no requirement for the matrix to be symmetric positive definite, making CGS ideal for solving the linear equation in Eq. (18).

After solving the Z-vector equation, the gradient vector of $\mathscr{E}_{\gamma}^{[\phi]}$ with respect to the nuclear displacement ξ can be computed as:

$$
\begin{aligned}
\frac{\mathrm{d}\mathscr{E}_{\gamma}^{[\phi]}}{\mathrm{d}\xi} &= \frac{\partial \mathscr{L}_{\gamma}^{[\phi]}}{\partial \xi} \\
&= \sum_{p,q} D_{p,q}^{\gamma,\text{var}} \frac{\partial h_{p,q}}{\partial \xi} + \sum_{p,q,r,s} d_{p,q,r,s}^{\gamma,\text{var}} \frac{\partial g_{p,q,r,s}}{\partial \xi} - \sum_{p,q} F_{p,q}^{\gamma,\text{eff}} \frac{\partial S_{p,q}}{\partial \xi} + \frac{\partial E_{\text{nuc}}}{\partial \xi} \\
&\quad - \sum_{p,q} \sum_i \left[D_{p,q}^{\gamma,\text{var}} Q_i^{[\phi]} + D_{p,q}^{[\phi]} \left(Q_i^{\text{e},\gamma,\text{var}} - Q_i^{\text{e},[\phi]} \right) \right] \frac{\partial}{\partial \xi} \left\langle p \left| \frac{1}{|\mathbf{r} - \mathbf{r}_i|} \right| q \right\rangle + \sum_i \frac{\partial V_i^{\text{N}}}{\partial \xi} Q_i^{\gamma,\text{var}} \\
&\quad + (\mathbf{Q}^{\text{e},\gamma,\text{var}})^\top \frac{\partial \mathbf{C}}{\partial \xi} \mathbf{Q}^{[\phi]} - \frac{1}{2} \left(\mathbf{Q}^{\text{e},[\phi]} \right)^\top \frac{\partial \mathbf{C}}{\partial \xi} \mathbf{Q}^{\text{e},[\phi]} + \frac{1}{2} \left(\mathbf{Q}^{\text{N}} \right)^{\text{T}} \frac{\partial \mathbf{C}}{\partial \xi} \mathbf{Q}^\top
\end{aligned} \tag{19}
$$

Here, $h_{p,q}$ and $g_{p,q,r,s}$ are the one-electron and electron repulsion (two-electron) integrals, respectively, and $S_{p,q}$ is the overlap matrix in the MO basis. The auxiliary (variational) density is given by:

$$
D_{p,q}^{\gamma,\text{var}} = D_{p,q}^{\gamma} + D_{p,q}^{\text{orb}} + D_{p,q}^{\text{CI}} + \check{D}_{p,q}^{\text{CI}} \tag{20}
$$

$$
d_{p,q,r,s}^{\gamma,\text{var}} = d_{p,q,r,s}^{\gamma} + d_{p,q,r,s}^{\text{orb}} + d_{p,q,r,s}^{\text{CI}} + \check{d}_{p,q,r,s}^{\text{CI}} \tag{21}
$$

where $D_{p,q}^{\text{orb}}$, $D_{p,q}^{\text{CI}}$, $d_{p,q,r,s}^{\text{orb}}$, and $d_{p,q,r,s}^{\text{CI}}$ are identical to Eqs. (12), (13), (15), and (16) in Ref. 56.

12

The CI contribution from the internal state rotations can be computed with the transition density matrix:

$$\check{D}_{p,q}^{\text{CI}} = \sum_{\eta > \pi \in \mathscr{P}} \omega_\gamma \overline{P}_{\eta,\pi}^{\gamma,[\phi]} \left\langle \Psi_\eta^{(0)} \left| \hat{E}_{p,q} + \hat{E}_{q,p} \right| \Psi_\pi^{(0)} \right\rangle \tag{22}$$

$$\check{d}_{p,q,r,s}^{\text{CI}} = \frac{1}{2} \sum_{\eta > \pi \in \mathscr{P}} \omega_\gamma \overline{P}_{\eta,\pi}^{\gamma,[\phi]} \left\langle \Psi_\eta^{(0)} \left| \hat{e}_{p,q,r,s} + \hat{e}_{p,q,s,r} + \hat{e}_{q,p,r,s} + \hat{e}_{q,p,s,r} \right| \Psi_\pi^{(0)} \right\rangle \tag{23}$$

for the target state γ. $\hat{E}_{p,q}$ and $\hat{e}_{p,q,r,s}$ are the one- and two-electron spin-averaged excitation operators, respectively. The effective Fock matrix is:

$$F_{p,q}^{\gamma,\text{eff}} = \sum_t D_{p,t}^{\gamma,\text{var}} h_{q,t} + \sum_{r,s,t} d_{p,r,s,t}^{\gamma,\text{var}} g_{q,r,s,t} + \sum_t D_{p,t}^{[\phi]} \mathscr{V}_{q,t}^{\gamma,\text{var}} . \tag{24}$$

Thus, the derivative of the wavefunction parameters are not explicitly evaluated because the multipliers have been determined so that the Lagrangian satisfies Eq. (17). The last three terms in Eq. (19) account for the displacement of tesserae. In this study, the position of tesserae is allowed to move, and these terms are evaluated in each geometry optimization step. With C-PCM, no approximations are required for the evaluation.[57]

2.2.3 Minimum energy conical intersections

Chemical processes near conical intersections are fundamentally dynamic in nature,[58] and implicit solvation models that rely on the equilibrium model are not very suitable for including solvent effects. Nevertheless, having a method to incorporate these effects would be highly advantageous.

The energy defined in Eq. (11) or (14) is not suitable for the crossing region. The order of states is easily flipped near degeneracy, and the state-specific solvation model may exhibit discontinuities in the potential energy surface (PES). While OpenMolcas includes a feature that automatically selects the relevant state for applying solvent effects, the resulting energy remains non-invariant under rotations between crossing states, rendering the formulation unsuitable for exploring such regions. Therefore, an energy expression that remains invariant near degeneracy is required. To

13

address this issue, the state-averaged energy in this study is defined as:

$$\mathscr{E}_{\text{SA}}^{[\phi,\chi]} = \sum_{\gamma \in \mathscr{P}} \omega_\gamma \left\langle \Psi_\gamma^{(0)} \left| \hat{H}^{\text{vac}} + \hat{V}^{[\phi,\chi]} \right| \Psi_\gamma^{(0)} \right\rangle - \frac{1}{2} \sum_i V_i^{\text{e},[\phi,\chi]} Q_i^{\text{e},[\phi,\chi]} + \frac{1}{2} \sum_i V_i^{\text{N}} Q_i^{\text{N}} + E_{\text{nuc}} \quad (25)$$

for crossing between states ϕ and χ ($\in \mathscr{P}$), where $V_i^{[\phi,\chi]}$ is written as

$$V_i^{[\phi,\chi]} = \frac{1}{2} \left(V_i^{[\phi]} + V_i^{[\chi]} \right) \quad (26)$$

and the ASC $Q_i^{\text{e},[\phi,\chi]}$ is determined by solving the matrix equation (Eq. (1)) using this ESP. Consequently, both the ASC and ESP are computed as the average of states ϕ and χ. If the transition rate between these crossing states is significant in degenerate regions, the solute density can be approximated as the average of the two states, validating the definition of Eq. (26). For state ϕ, the state-specific energy is:

$$\mathscr{E}_\phi^{[\phi,\chi]} = \left\langle \Psi_\phi^{(0)} \left| \hat{H}^{\text{vac}} \right| \Psi_\phi^{(0)} \right\rangle + \frac{1}{2} \sum_i V_i^{[\phi,\chi]} Q_i^{[\phi,\chi]} + E_{\text{nuc}} \; . \quad (27)$$

For state χ, $\Psi_\phi^{(0)}$ is replaced by $\Psi_\chi^{(0)}$. The average of the state-specific energies for both crossing states can be expressed as:

$$\begin{aligned}
\mathscr{G}_{\phi\chi}^{[\phi,\chi]} &= \frac{1}{2} \left(\mathscr{E}_\phi^{[\phi,\chi]} + \mathscr{E}_\chi^{[\phi,\chi]} \right) \\
&= \left\langle \frac{1}{2} \left(\Psi_\phi^{(0)} + \Psi_\chi^{(0)} \right) \left| \hat{H}^{\text{vac}} \right| \frac{1}{2} \left(\Psi_\phi^{(0)} + \Psi_\chi^{(0)} \right) \right\rangle + \frac{1}{2} \sum_i V_i^{[\phi,\chi]} Q_i^{[\phi,\chi]} + E_{\text{nuc}} \; . \quad (28)
\end{aligned}$$

The (free) energies for ϕ and χ, defined in this manner, are invariant with respect to rotations between the two states (though not for others). This invariance is crucial for ensuring smooth PESs (and convergence of SCF) in the vicinity of crossing regions.

To find (minimum energy) CoIns, we usually compute the gradient difference and non-adiabatic

coupling (NAC) vectors:

$$g_\xi^{\phi,\chi} = \frac{\mathrm{d}\mathscr{E}_\chi^{[\phi,\chi]}}{\mathrm{d}\xi} - \frac{\mathrm{d}\mathscr{E}_\phi^{[\phi,\chi]}}{\mathrm{d}\xi} \tag{29}$$

$$h_\xi^{\phi,\chi} = \left\langle \Psi_\phi^{(0)} \left| \frac{\mathrm{d}\left(\hat{H}^{\mathrm{vac}} + \hat{V}^{[\phi,\chi]}\right)}{\mathrm{d}\xi} \right| \Psi_\chi^{(0)} \right\rangle \tag{30}$$

The gradient difference vector $\mathbf{g}^{\phi,\chi}$ can be derived as shown in previous sections. On the other hand, the NAC vector $\mathbf{h}^{\phi,\chi}$ requires a slight adjustment to the right-hand side of Eq. (11). Specifically, instead of the free energy, we use $\langle \Psi_\phi^{(0)} | \hat{H}^{\mathrm{vac}} + \hat{V}^{[\phi,\chi]} | \Psi_\chi^{(0)} \rangle$. This requires omitting the last three terms in Eq. (11). The Lagrangian can be generalized as follows:

$$
\begin{aligned}
\mathscr{L}_{\alpha\beta}^{[\phi,\chi]} = {} & \left\langle \Psi_\alpha^{(0)} \left| \hat{H}^{\mathrm{vac}} + \hat{V}^{[\phi,\chi]} \right| \Psi_\beta^{(0)} \right\rangle \\
& + \delta_{\alpha,\beta} \left(-\frac{1}{2} \sum_i V_i^{\mathrm{e},[\phi,\chi]} Q_i^{\mathrm{e},[\phi,\chi]} + \frac{1}{2} \sum_i V_i^{\mathrm{N}} Q_i^{\mathrm{N}} + E_{\mathrm{nuc}} \right) \\
& + \sum_{p,q} \overline{\kappa}_{p,q}^{\alpha\beta,[\phi,\chi]} \frac{\partial \widetilde{\mathscr{E}}_{\mathrm{SA}}^{[\phi,\chi]}}{\partial \kappa_{p,q}} + \sum_{\eta \in \mathscr{P}} \sum_{\pi > \eta} \overline{P}_{\eta,\pi}^{\alpha\beta,[\phi,\chi]} \frac{\partial \widetilde{\mathscr{E}}_{\mathrm{SA}}^{[\phi,\chi]}}{\partial P_{\eta,\pi}} ,
\end{aligned}
\tag{31}
$$

where $\delta_{\alpha,\beta}$ is the Kronecker delta. The rest of the calculation is quite similar to the gradient of $\mathscr{E}_\gamma^{[\phi]}$.

Since the definition of the ESP is inconsistent when finding equilibrium (single state) and MECoIn (averaged over crossing states) structures, PESs may not connect smoothly. However, as this study focuses on specific stationary points (with few exceptions), this issue is not of immediate concern. In cases such as molecular dynamics simulations, where surface hopping events are investigated, a weighted average solvation approach may prove useful.[27]

2.3 CASPT2/PCM

As long as the coupling between the CASPT2 density and the solvent is ignored, extending the method to CASPT2 is straightforward. The reaction field is determined at the SCF level, and

15

during the PT2 calculation, the solvent effect is fixed and included in a perturbative manner. This approach is similar to that described in Ref. 59 and corresponds to the PTE approach.[39] Although the solvent reaction field remains fixed during the PT2 calculation in this study as well, it is possible to relax the solvent after obtaining the fully relaxed (or unrelaxed) density matrix. The impact of this relaxation on the energetics is discussed in Section 4.3.2.

2.3.1 CASPT2/PCM energy

In CASPT2, we first define the generalized Fock operator as:

$$
\begin{aligned}
\hat{F}^{\gamma,[\phi]} &= \sum_{p,q} f_{p,q}^{\gamma,[\phi]} \hat{E}_{p,q} \\
&= \sum_{p,q} \left(h_{p,q} + \mathscr{V}_{p,q}^{[\phi]} + \sum_{r,s} \left[g_{p,q,r,s} - \frac{1}{2} g_{p,r,q,s} \right] D_{r,s}^{\gamma} \right) \hat{E}_{p,q}
\end{aligned} \tag{32}
$$

The solute density used in the third term of Eq. (32) is independent of the density that polarized the solvent, being determined solely by the selected CASPT2 model. Next, the zeroth-order Hamiltonian for MS-CASPT2 is typically defined as:

$$
\begin{aligned}
\hat{H}_{\gamma}^{(0),[\phi]} &= \sum_{\gamma \in \mathscr{P}} |\Psi_{\gamma}^{(0)}\rangle \langle \Psi_{\gamma}^{(0)} | \hat{F}^{\gamma,[\phi]} | \Psi_{\gamma}^{(0)} \rangle \langle \Psi_{\gamma}^{(0)} | \\
&+ \sum_{k \in \mathscr{P}^{\perp}} |\Psi_{k}^{(0)}\rangle \langle \Psi_{k}^{(0)} | \hat{F}^{\gamma,[\phi]} | \Psi_{k}^{(0)} \rangle \langle \Psi_{k}^{(0)} | \\
&+ \hat{Q}_{\mathrm{SD}}^{\gamma} \hat{F}^{\gamma,[\phi]} \hat{Q}_{\mathrm{SD}}^{\gamma} + \hat{Q}_{\mathrm{TQ}\cdots}^{\gamma} \hat{F}^{\gamma,[\phi]} \hat{Q}_{\mathrm{TQ}\cdots}^{\gamma}
\end{aligned} \tag{33}
$$

$\hat{Q}_{\mathrm{SD}}^{\gamma}$ and $\hat{Q}_{\mathrm{TQ}\cdots}^{\gamma}$ project onto the first-order and higher-order interacting spaces, respectively. If the extended-type MS-CASPT2 methods, extended multistate (XMS-),[60] extended dynamically weighted (XDW-),[61] and rotated multistate (RMS-),[62] are employed, the rotated reference states $\widetilde{\Psi}_{\gamma}^{(0)}$ that satisfy:

$$
\langle \widetilde{\Psi}_{\gamma}^{(0)} | \hat{F}^{\mathrm{SA},[\phi]} | \widetilde{\Psi}_{\eta}^{(0)} \rangle = 0 \tag{34}
$$

16

for $\gamma \neq \eta \in \mathscr{P}$ are used instead of the (unrotated) reference states $\Psi_\gamma^{(0)}$. The key difference between the XMS-, XDW-, and RMS-CASPT2 methods lies in how the generalized Fock operator (Eq. (32)) is defined. XMS- uses the equally state-averaged density matrix, XDW- uses a dynamically weighted average, and RMS- employs a state-specific density matrix. To compute the second-order perturbation energy, the first-order correction to the wavefunction $\Psi_\gamma^{(1)}$ is required, expressed as a linear combination of doubly excited configurations from the reference state:

$$|\Psi_\gamma^{(1)}\rangle = \sum_{p,q,r,s} T_{p,q,r,s}^\gamma \hat{E}_{p,q} \hat{E}_{r,s} |\widetilde{\Psi}_\gamma^{(0)}\rangle \tag{35}$$

The excitation amplitude $T_{p,q,r,s}^\gamma$ is iteratively determined by solving the linear equation

$$\langle \Phi_{p,q,r,s} | \hat{H}^{\mathrm{vac}} + \hat{V}^{[\phi]} | \widetilde{\Psi}_\gamma^{(0)}\rangle + \langle \Phi_{p,q,r,s} | \hat{H}_\gamma^{(0),[\phi]} - E_\gamma^{(0),[\phi]} + E_{\mathrm{shift}} | \Psi_\gamma^{(1)}\rangle = 0 \,, \tag{36}$$

where $|\Phi_{p,q,r,s}\rangle$ is the doubly excited configuration, $E_\gamma^{(0),[\phi]}$ is the zeroth-order energy, and E_{shift} is the term that comes from the real or imaginary shift to avoid the intruder state problem.

The (electronic) MS-CASPT2 energy is then obtained by diagonalizing the effective Hamiltonian $H_{\eta,\theta}^{\mathrm{eff},[\phi]}$:

$$\begin{aligned} \overline{H}_{\eta,\theta}^{\mathrm{eff},[\phi]} &= \langle \widetilde{\Psi}_\eta^{(0)} | \hat{H}^{\mathrm{vac}} + \hat{V}^{[\phi]} | \widetilde{\Psi}_\theta^{(0)}\rangle - \frac{1}{2} \sum_i V_i^{\mathrm{e},[\phi]} Q_i^{\mathrm{e},[\phi]} \delta_{\eta,\theta} \\ &\quad + \frac{1}{2} \left(\langle \widetilde{\Psi}_\eta^{(0)} | \hat{H}^{\mathrm{vac}} + \hat{V}^{[\phi]} | \Psi_\theta^{(1)}\rangle + \langle \widetilde{\Psi}_\theta^{(0)} | \hat{H}^{\mathrm{vac}} + \hat{V}^{[\phi]} | \Psi_\eta^{(1)}\rangle \right) \end{aligned} \tag{37}$$

The first term is the sum of the zeroth- and first-order energies of the rotated reference state, and the second term is the free energy correction determined at the SCF level. The third term is evaluated at the PT2 level, using the first-order correction to the wavefunction $\Psi_\eta^{(1)}$. Since the free energy correction term (the second term in Eq. (37)) applies to all internal states, the unitary transformation of $\overline{H}_{\eta,\theta}^{\mathrm{eff},[\phi]}$ leads to the original free energy correction. This means that the free energy correction at the MS-CASPT2 level is equivalent to that at the SA-MCSCF level. Consequently, the MS-

17

CASPT2 energy is expressed with the rotation matrix $R_{\eta,\theta}$ that diagonalizes $H_{\eta,\theta}^{[\phi],\mathrm{eff}}$:

$$
\begin{aligned}
\mathscr{E}_{\gamma}^{\mathrm{CASPT2},[\phi]} &= \sum_{\eta,\theta\in\mathscr{P}} R_{\eta,\gamma}\overline{H}_{\eta,\theta}^{\mathrm{eff},[\phi]} R_{\theta,\gamma} - \frac{1}{2}\sum_{i} V_i^{\mathrm{e},[\phi]} Q_i^{\mathrm{e},[\phi]} + \frac{1}{2}\sum_{i} V_i^{\mathrm{N}} Q_i^{\mathrm{N}} + E_{\mathrm{nuc}} \\
&= E_{\gamma}^{\mathrm{CASPT2}} + \sum_{i} V_i^{\mathrm{e},[\gamma],\mathrm{PT2}} Q_i^{[\phi]} - \frac{1}{2}\sum_{i} V_i^{\mathrm{e},[\phi]} Q_i^{\mathrm{e},[\phi]} + \frac{1}{2}\sum_{i} V_i^{\mathrm{N}} Q_i^{\mathrm{N}} + E_{\mathrm{nuc}} \\
&\approx E_{\gamma}^{\mathrm{CASPT2}} + \frac{1}{2}\sum_{i} V_i^{[\phi]} Q_i^{[\phi]} + E_{\mathrm{nuc}} \; .
\end{aligned}
\tag{38}
$$

$E_{\gamma}^{\mathrm{CASPT2}}$ is the electronic CASPT2 energy, and the electrostatic contribution $V_i^{\mathrm{e},[\gamma],\mathrm{PT2}}$ is the ESP from the unrelaxed density matrix at the PT2 level (including the density at the SCF level). The final approximation holds when $\gamma = \phi$ and the perturbed state γ after the rotation is predominantly characterized by ϕ ($V_i^{\mathrm{e},[\gamma],\mathrm{PT2}} \approx V_i^{\mathrm{e},[\phi]}$). This condition is typically satisfied if the state γ is energetically non-degenerate, with exceptions occurring near CoIn. In such cases, the density of the crossing states must be averaged, as discussed in Section 2.2.3. Although degeneracies at the CASPT2 level do not necessarily correspond to degeneracies at the SCF level, the reaction field is generated based on the average of the SCF-determined densities.

Therefore, energy calculations and geometry optimizations at the CASPT2/PCM level should be performed exclusively for $\gamma = \phi$. Note that γ and ϕ are determined by the character of the state rather than its energetic order, which may differ at the SCF and PT2 levels. Consequently, the RFROOT and RLXROOT keywords must be specified separately in the input file to define ϕ and γ, respectively.

2.3.2 CASPT2/PCM gradients

The analytic derivatives of MS-CASPT2 variants can be computed following the approach outlined in Ref. 63. We begin by defining the PT2 Lagrangian for state γ as:

$$
\begin{aligned}
\mathscr{L}_{\gamma,\alpha\beta}^{\mathrm{PT2},[\phi]} = {} & \frac{1}{2} \sum_{\eta \in \mathscr{P}} \overline{H}_{\gamma,\eta}^{\mathrm{eff},[\phi]} \left(R_{\gamma,\alpha} R_{\eta,\beta} + R_{\gamma,\beta} R_{\eta,\alpha} \right) \\
& + \sum_{p,q,r,s} \overline{\lambda}_{p,q,r,s}^{\gamma,\alpha\beta} \left(\left\langle \Phi_{p,q,r,s}^{\gamma} | \hat{H}^{\mathrm{vac}} + \hat{V}^{[\phi]} | \widetilde{\Psi}_{\gamma}^{(0)} \right\rangle + \left\langle \Phi_{p,q,r,s}^{\gamma} | \hat{H}_{\gamma}^{[\phi],(0)} - E_{\gamma}^{[\phi],(0)} + E_{\mathrm{shift}} | \Psi_{\gamma}^{(1)} \right\rangle \right)
\end{aligned}
\tag{39}
$$

Additional terms may be required if frozen core approximations[64] and/or ionization potential–electron affinity (IPEA) shift[65] are applied. The first term in Eq. (39) represents the (electronic) energy to be differentiated, and the second term is the constraint condition for determining the excitation amplitude (Eq. (36)). Since this energy is not obtained through a variational minimization with respect to the excitation amplitudes (and wavefunction parameters), we first need to solve the following λ-equation for each γ:

$$
\frac{\partial \mathscr{L}_{\gamma,\alpha\beta}^{\mathrm{PT2}}}{\partial T_{p,q,r,s}^{\gamma}} = 0
\tag{40}
$$

to determine $\overline{\lambda}_{p,q,r,s}^{\gamma,\alpha\beta}$. Since the reaction field is fixed during the PT2 calculation, there is no need for PCM-related computations during the CASPT2 calculation. Next, we need to define the total PT2 Lagrangian:

$$
\mathscr{L}_{\alpha\beta}^{\mathrm{PT2},[\phi]} = \sum_{\gamma \in \mathscr{P}} \mathscr{L}_{\gamma,\alpha\beta}^{\mathrm{PT2},[\phi]} + \sum_{\gamma > \eta \in \mathscr{P}} \overline{\omega}_{\gamma,\eta}^{\alpha\beta,[\phi]} \left\langle \widetilde{\Psi}_{\gamma}^{(0)} \left| \hat{F}^{\mathrm{SA},[\phi]} \right| \widetilde{\Psi}_{\eta}^{(0)} \right\rangle .
\tag{41}
$$

The second term comes from the constraint condition for the extended MS-CASPT2 (Eq. (34)), and the Lagrange multiplier $\overline{\omega}_{\gamma,\eta}^{\alpha\beta,[\phi]}$ can be determined non-iteratively, as described in Ref. 63. After this, we solve the Z-vector equation:

$$
\frac{\partial \mathscr{L}_{\alpha\beta}^{\mathrm{CASPT2},[\phi]}}{\partial \kappa_{p,q}} = \frac{\partial \mathscr{L}_{\alpha\beta}^{\mathrm{CASPT2},[\phi]}}{\partial P_{\eta,\pi}} = 0
\tag{42}
$$

19

where

$$\begin{aligned}
\mathscr{L}_{\alpha\beta}^{\mathrm{CASPT2},[\phi]} &= \mathscr{L}_{\alpha\beta}^{\mathrm{PT2},[\phi]} + \mathscr{L}_{\alpha\beta}^{\mathrm{SCF},[\phi]} \\
&+ \delta_{\alpha,\beta}\left(-\frac{1}{2}\sum_i V_i^{\mathrm{e},[\phi]}Q_i^{\mathrm{e},[\phi]} + \frac{1}{2}\sum_i V_i^{\mathrm{N}}Q_i^{\mathrm{N}} + E_{\mathrm{nuc}}\right).
\end{aligned} \tag{43}$$

The remaining computation is similar to the SA-MCSCF/PCM case (Section 2.2.2), and the total derivative of the CASPT2 energy can be computed as a partial derivative of the Lagrangian:

$$\frac{\mathrm{d}\mathscr{E}_{\alpha\beta}^{\mathrm{CASPT2},[\phi]}}{\mathrm{d}\xi} = \frac{\partial\mathscr{L}_{\alpha\beta}^{\mathrm{CASPT2},[\phi]}}{\partial\xi} \tag{44}$$

Analytic derivatives of the RASPT2 energy can be obtained similarly, as shown in Ref. 64. The extension to the NAC vector is also analogous to the SA-MCSCF/PCM case.

In principle, computing analytic gradients requires evaluating the relaxed density. Thus, it is possible to include solvent effects using the CASPT2 density (PTED approach). However, this would require evaluating the relaxed density multiple times during each geometry optimization step, making it impractical for realistic molecular systems.

2.4   Equilibrium and non-equilibrium solvation

The electron (de)excitation process occurs rapidly, while the relaxation (reorganization) of solvent molecules is relatively slow. When both the electron and molecular configurations are fully relaxed in a given state, this is referred to as the equilibrium regime. However, the geometrical relaxation of solvent molecules does not happen instantaneously and cannot keep pace with the absorption or emission processes. To account for the different timescales, we separate the fast and slow components: only the fast component responds to the (de)excited state, while the slow component is constructed using the reaction field of the initial state. This situation is described as a non-equilibrium regime.

In OpenMolcas, the Marcus partition scheme (Partition I, see Table 2 in Ref. 17) is used. A

similar (equivalent if C-PCM is applied[66]) formulation exists, known as the Pekar partition. First, we calculate the solvent charge in the initial state (init) $\mathbf{Q}_{\text{init}}$, which is treated as the slow (orientational or inertial) component: $\mathbf{Q}_{\text{init}}^{\text{slow}} = (\varepsilon - \varepsilon^{\infty})\mathbf{Q}_{\text{init}}/(\varepsilon - 1)$, where ε^{∞} is the optical dielectric constant. Then, during the calculation for the final state, the electrostatic potential on each tessera $\mathbf{V}_{\text{final}}$ is computed in the presence of the fixed $\mathbf{Q}_{\text{init}}^{\text{slow}}$. The fast component of the ASC at the final state $\mathbf{Q}_{\text{final}}^{\text{fast}}$ is obtained by solving Eq. (1) using $\mathbf{V}_{\text{final}}$ and ε^{∞} instead of ε. The density used for obtaining $\mathbf{Q}_{\text{init}}^{\text{slow}}$ and $\mathbf{Q}_{\text{final}}^{\text{fast}}$ can be determined at either the SCF or PT2 level. The SCF density is directly obtained as a result of solving the SCF equation, while the PT2 density must be found iteratively by solving the SCF and PT2 equations, as done in the PTED approach. Since using the PT2 density is impractical, the SCF density is used for computing non-equilibrium energies as well.

3 Computational Details

The theory outlined in the previous section has been implemented in a development version of OpenMolcas. The latest version of the developed code and example files can be found on GitHub (https://github.com/YoshioNishimoto/Some-Developments-with-OpenMolcas) All CASSCF and CASPT2 results were obtained using this version, which utilizes atomic compact Cholesky decomposition[67,68] to generate on-the-fly auxiliary basis sets for the resolution-of-the-identity treatment of electron repulsion integrals. All CASPT2 calculations employed the frozen core approximation, and the IPEA shift parameter[69] was set to 0.00 unless otherwise noted. Symmetry constraints were not applied, and Löwdin's canonical orthonormalization was used to orthonormalize the internally contracted basis. A recently introduced gradient-enhanced Kriging approach[70–72] was applied to locate stationary points. Nearly all PCM options were used as defaults, except that the "COND" (conductor-PCM) and "PAUL" (Pauling atomic radii) options were explicitly activated.

First, the accuracy of the implemented gradient and the smoothness of the potential energy

21

surface (PES) are examined using acrolein in water. The reference wavefunctions were obtained at the three-state-averaged (SA3)-CASSCF(6e,5o) level, where the active space consisted of six electrons in five orbitals. CASPT2 calculations were carried out with an imaginary level shift[73] of 0.2i.

The performance of the developed method for stationary points and MECoIn was tested with the protonated Schiff-base (PSB3) in both vacuum and MeOH (methanol). To compare with previous CASSCF and MS-CASPT2 results using RISM,[32] the reference wavefunction was obtained at the SA3-CASSCF(6e,6o) level (six π orbitals) with the 6-31G(d) basis set.[74,75] As it is well known that PESs of MS-CASPT2 near crossing regions can show discontinuities,[76] RMS-CASPT2 was used to investigate the topography of CoIns. For consistency with previous studies, a real level shift of 0.3 was employed.

To further evaluate the method, absorption energies of *para*-nitroaniline were computed in vacuum, cyclohexane, toluene, dichloroethane, acetonitrile, and water. The reference SCF calculations were performed using a CAS(16e,12o) active space, consisting of ten π orbitals and two n_O orbitals (see Figure S1 in the Supporting Information). The first five states were equally averaged (SA5). Geometry optimizations and absorption energy calculations were performed at the CASSCF, XMS-CASPT2, and RMS-CASPT2 levels using the ANO-RCC-VTZP basis set.[77,78] CASPT2 calculations were conducted with an imaginary level shift of 0.2i.

4 Results and Discussion

4.1 Acrolein

4.1.1 Accuracy of Analytic Gradients

The accuracy of the implemented analytic gradient was tested by comparing it with numerical gradients for (*s-trans*) acrolein in water, calculated at the CASSCF, XMS-CASPT2, and RMS-CASPT2 levels of theory. The geometry was initially optimized at the Hartree–Fock level us-

ing the cc-pVDZ basis set[79] in vacuum. The reference SCF calculations were performed with SA3-CASSCF(6e,5o)/cc-pVDZ (four π orbitals and one n_O orbital), with the solvent charge polarized according to the state for which gradients were calculated. Since the energy computed with PCM is translationally invariant but not rotationally (due to discrete tesserae), numerical gradients were obtained by differentiating in Cartesian coordinates with a displacement parameter of 5.0×10^{-4} bohr. The root-mean-square (RMS) deviation is summarized in Table 1. The differences for CASSCF and CASPT2 across all states were on the order of 10^{-6} hartree bohr^{-1}, which is sufficiently accurate in practice.

Table 1: Root-mean-square (RMS) differences between analytic and numerical gradients (unit in hartree bohr^{-1}), with the SA3-CAS(6e,5o)/cc-pVDZ reference.

	CASSCF	XMS-CASPT2	RMS-CASPT2
S_0	1.76×10^{-6}	1.14×10^{-6}	1.59×10^{-6}
S_1	1.72×10^{-6}	4.76×10^{-6}	5.08×10^{-6}
S_2	1.52×10^{-6}	4.83×10^{-6}	5.07×10^{-6}

4.1.2 Smoothness of the PES

The smoothness of the PES was tested using the reference wavefunction from SA3-CASSCF(6e,5o)/cc-pVDZ. PESs for S_0 and S_1 near a MECoIn at the XMS-CASPT2 level are shown in Figure 1 (a). Corresponding figures for CASSCF and RMS-CASPT2 and **x** and **y** vectors for all levels are provided in Figures S2 and S3, respectively, in the Supporting Information. In Figure 1, **x** and **y** represent linear combinations of the (orthonormalized) gradient difference and NAC vectors, with displacement along these vectors lifting the degeneracy. The **x** and **y** approximately correspond to in-plane and out-of-plane modes, respectively. The $\mathscr{P}^{\mathrm{CoIn}}$ and $\mathscr{B}^{\mathrm{CoIn}}$ parameters[56] are summarized in Table 2. The relatively large $\mathscr{P}^{\mathrm{CoIn}}$ values ($\mathscr{P}^{\mathrm{CoIn}} > 1$) indicate that these MECoIns are strongly sloped, which is evident from the steeply tilted PESs in Figure 1 (a). The $\mathscr{B}^{\mathrm{CoIn}}$ values, which classify conical intersections as bifurcating or single-path, are all greater than one, signify-

23

ing that these are single-path conical intersections, implying the local topography directs toward a single product. Comparing these parameters in vacuum and water, the solvent effect does not significantly impact the local topography in this example. Figure 1 (b) shows the XMS-CASPT2 energy difference between S_0 and S_1 around the CASSCF MECoIn. Since the CASSCF energy is made invariant with respect to rotations between crossing states (Eq. (28)), and XMS-CASPT2 are strictly invariant to such rotations in the model space (except for minor non-invariance in the first-order interacting space), the PESs at the CASPT2 level with PCM are smooth.
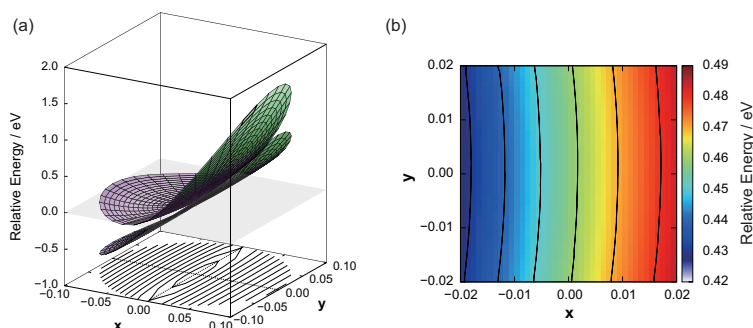

Figure 1: (a) XMS-CASPT2 PESs of acrolein around the S_0/S_1 MECoIn obtained at the XMS-CASPT2 level, and (b) XMS-CASPT2 energy differences around the S_0/S_1 MECoIn at the CASSCF level, with the SA3-CAS(6e,5o)/cc-pVDZ reference.

Table 2: $\mathscr{P}^{\text{CoIn}}$ and $\mathscr{B}^{\text{CoIn}}$ values of the S_0/S_1 MECoIn of acrolein.

	Vacuum		PCM (water)	
	$\mathscr{P}^{\text{CoIn}}$	$\mathscr{B}^{\text{CoIn}}$	$\mathscr{P}^{\text{CoIn}}$	$\mathscr{B}^{\text{CoIn}}$
CASSCF	14.37	2.46	15.77	2.54
XMS-CASPT2	4.55	1.68	4.71	1.70
RMS-CASPT2	4.85	1.72	4.92	1.73

It should be noted that the discontinuities discussed in this study are strictly related to the electronic structure. PCM introduces other sources of discontinuity, such as the creation and annihilation of tesserae[80] and electrostatic interactions between tesserae,[81] which are beyond the scope of this study.

4.2 Protonated Schiff-Base

Next, a comparison between RISM calculations[32] in vacuum and MeOH was carried out for the protonated Schiff base (PSB3; $C_5H_6NH_2^+$), using a reference wavefunction of SA3-CASSCF(6e,6o)/6-31G(d). The relative energies of three stationary points are summarized in Table 3. The "FC" entry corresponds to the energy of the Franck–Condon geometry (planar) in the ground state, "SP" refers to the energy of the saddle point (planar) in the first excited state, and "$(CCT)_{CoIn}$" represents the S_0/S_1 MECoIn around the C–C twisting coordinate. The optimized coordinates can be found in the Supporting Information. Although the CASSCF results in vacuum were mostly reproduced, the MS-CASPT2 results were already poorly reproduced in vacuum. The MS-CASPT2 calculations in this study and Ref. 32 were performed using different software packages, and there were some technical differences (e.g., internal contractions, electron repulsion integrals, and spatial symmetry), making direct comparison difficult. Nonetheless, we observe that the computed relative energies in this study systematically underestimate the values for FC and $(CCT)_{CoIn}$, suggesting that qualitative discussion for these entries is possible. However, the discrepancy for SP is notably large.

Table 3: Relative energies of PSB3 (unit in eV) with the SA3-CAS(6e,6o)/6-31G(d) reference. Values in parentheses are from Ref. 32, where the solvent effect is treated using RISM.

	CASSCF			MS-CASPT2		
	FC	SP	$(CCT)_{CoIn}$	FC	SP	$(CCT)_{CoIn}$
			Vacuum			
S_2	5.739 (5.73)	5.569 (5.57)	6.629 (6.42)	5.252 (5.44)	4.906 (5.36)	5.787 (5.99)
S_1	5.031 (5.01)	4.605 (4.60)	3.213 (3.25)	4.083 (4.28)	3.915 (3.86)	2.428 (2.60)
S_0	0.000 (0.00)	0.847 (0.85)	3.213 (3.25)	0.000 (0.00)	0.163 (0.34)	2.428 (2.60)
			MeOH			
S_2	6.116 (5.99)	5.875 (5.80)	6.846 (6.66)	5.669 (6.00)	5.155 (5.60)	5.917 (6.10)
S_1	5.815 (5.71)	4.928 (4.86)	3.543 (3.26)	4.649 (4.09)	4.153 (3.86)	2.645 (2.67)
S_0	0.000 (0.00)	0.866 (1.05)	3.543 (3.26)	0.000 (0.00)	0.394 (0.21)	2.645 (2.67)

For the CASSCF results, we find that the trend of solvent-induced shifts is generally reproduced by PCM, though the shifts are overestimated by 0.1–0.2 eV for most entries. A significant excep-

25

tion is found for $(CCT)_{CoIn}$: the RISM calculation in Ref. 32 showed a minimal energetic shift (0.01 eV) due to the solvent, while PCM predicted a shift of 0.33 eV in this study. This discrepancy could be due to PCM systematically overestimating the shift or differences in the treatment of the solvent near the CoIn. The present study assumes full equilibration of the solvent, with polarization based on the averaged density of the crossing states. In contrast, the RISM calculation in Ref. 32 used a non-equilibrium model in a linear-response fashion.[31] The equilibrium regime allows more degrees of freedom (e.g., solvent coordinates) to relax, leading to greater stabilization when the system equilibrates. If the deviation arises primarily from the different treatment of equilibration, we expect that PCM overestimates the stabilization and thus predicts lower relative energies than the systematic shift. However, the observed shift is quite similar. Another potential consequence of the differing equilibration regimes is that averaging the density matrices of the two states may partially cancel out the ESP from the solute, reducing the polarization of the ASC and thus the stabilization of the solute. While the dipole moment of charged systems is not uniquely defined, the dipole moments of the crossing states point in similar directions, meaning that this ESP cancellation should not be significant. The reason for the discrepancy of $(CCT)_{CoIn}$ is not clear at the moment, but overall, solvent effects are qualitatively captured by PCM at the CASSCF level, though improvements are needed, particularly in describing the crossing regions.

Since the CASPT2 results in vacuum are already significantly different, direct comparison between the two solvation models is challenging. Nevertheless, considering that the solvent effect on FC is qualitatively captured at the CASSCF level, the discrepancy should largely be attributed to differences in the CASPT2 implementation. One interesting observation is the shift in S_1 energy for FC: RISM predicts a redshift, while PCM predicts a blueshift, consistent with CASSCF results. This contradictory finding suggests that dynamical electron correlation effects depend significantly on the solvation model, but further analysis is difficult given the inherent differences in the CASPT2 calculations.

Despite these differences, the local topography of the $(CCT)_{CoIn}$ in vacuum and MeOH is compared in Figure 2. To mitigate the non-invariance issue of the MS-CASPT2 method, RMS-

26

CASPT2 was employed for subsequent analysis. The $\mathbf{x}$ and $\mathbf{y}$ (see page S-9 and Figure S4 in the Supporting Information) approximately correspond to C–C stretching mode adjacent to the amino group and the torsional mode around the C–C bond, respectively. The $\mathscr{P}^{\text{CoIn}}$ value is 4.11×10^{-3} in vacuum and 0.40 in MeOH, indicating that the CoIn is locally peaked in both environments. The smaller value of $\mathscr{P}^{\text{CoIn}}$ in vacuum suggests that the CoIn could be a more efficient funnel. The $\mathscr{B}^{\text{CoIn}}$ value is 0.48 in vacuum and 1.27 in MeOH, indicating that the *local* topography of the CoIn leads to two products in vacuum and one product in MeOH after relaxation. The potential energy curve (PEC) for a displacement of 0.01 from the MECoIn point (in terms of normalized $\mathbf{x}$ and $\mathbf{y}$) is compared in Figure 3. The horizontal axis corresponds to the rotation angle between $\mathbf{x}$ and $\mathbf{y}$, and the displacement from the MECoIn structure is given by $0.01(\mathbf{x} \cdot \sin\theta + \mathbf{y} \cdot \cos\theta)$. The dot products of $\mathbf{x}$ and $\mathbf{y}$ in vacuum and MeOH indicate that these vectors are almost parallel ($\mathbf{x}_{\text{vac}} \cdot \mathbf{x}_{\text{MeOH}} = 0.964$ and $\mathbf{y}_{\text{vac}} \cdot \mathbf{y}_{\text{MeOH}} = 0.996$).
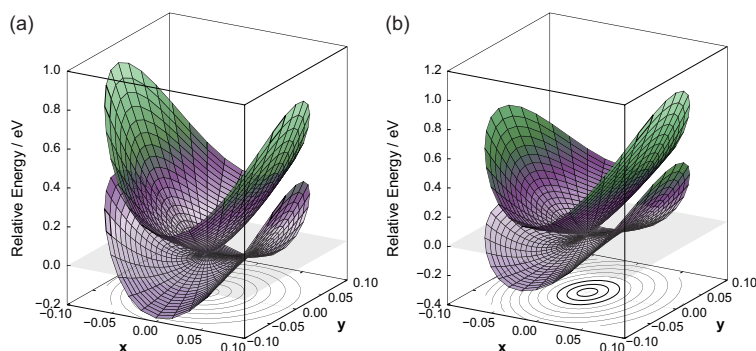

Figure 2: (SA3-)RMS-CASPT2(6e,6o)/6-31G(d) PESs of PSB3 around the (CCT)$_{\text{CoIn}}$ in (a) vacuum and (b) MeOH

Indeed, the lower-state PEC (S$_0$) indeed shows two shallow minima in vacuum, indicating a bifurcating intersection ($\mathscr{B}^{\text{CoIn}} < 1$), while only one minimum appears in MeOH, indicating a single-path intersection ($\mathscr{B}^{\text{CoIn}} > 1$). Minimum energy path (MEP) calculations from the two displaced geometries corresponding to the minima in vacuum on the S$_0$ PEC (($\mathbf{x},\mathbf{y}$) = (0.0034, 0.0094) and (0.0034, $-$0.0094)) lead to *trans*- and *cis*-PSB3, respectively. In contrast, there is only one minimum on the S$_0$ PEC in MeOH, and geometry optimization from the displaced geometry (($\mathbf{x},\mathbf{y}$) = ($-$0.0100, 0.0000)) leads to the *cis*-PSB3 structure, suggesting that solvent effects may
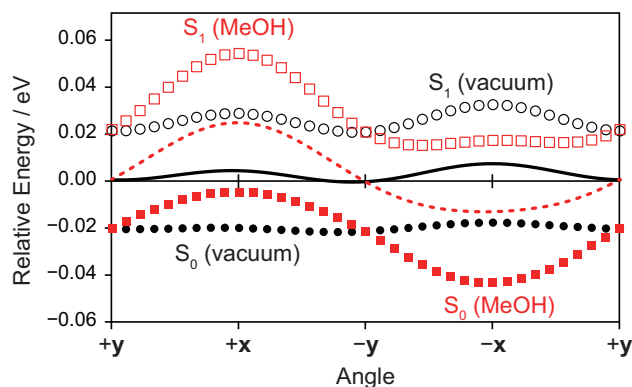
27

Figure 3: (SA3-)RMS-CASPT2(6e,6o)/6-31G(d) S_0 and S_1 PECs around the $(CCT)_{CoIn}$ at a distance of 0.01. The solid (vacuum) and dotted (MeOH) lines are the average of S_0 and S_1.

influence the product ratio after non-radiative decay. Note that the solvent reaction field during the MEP calculations was generated using an equally averaged density matrix over S_0 and S_1 at the SCF level, regardless of the energy difference between the two states.

4.3 *para*-Nitroaniline

Para-Nitroaniline (Figure 4) exhibits a charge-transfer-type excitation. Due to the significant change in dipole moment induced by charge-transfer excitations, this molecule is well-suited for evaluating the performance of the developed method. The reference SCF calculations were carried out using SA5-CAS(16e,12o), as the S_4 state represents a charge-transfer state with the reaction field of the S_0 state. However, when the reaction field is equilibrated with the charge-transfer state (in water), the S_4 state becomes greatly stabilized relative to other states, ultimately settling as S_1.
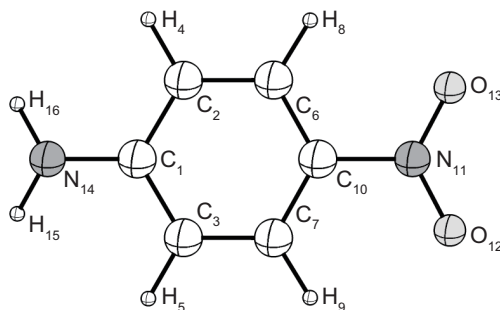

Figure 4: Structure of *para*-nitroaniline.

28

4.3.1 Geometrical parameters

We first compare geometrical parameters in vacuum with experimental results in crystal.[82] The comparison (Table 4) shows that discrepancies in CASSCF geometry are mitigated when using XMS- and RMS-CASPT2. For example, the error in the N_{11}–O_{12} bond (N–O in the nitro group) is reduced from 0.05 Å at the CASSCF level to 0.01 Å when dynamic electron correlation is included. Similarly, an improvement is observed for the C_1–N_{14} bond (between the amino group and benzene ring).

Table 4: Optimized bond distances of *para*-nitroaniline in vacuum (unit in Å) with the SA5-CAS(16e,12o)/ANO-RCC-VTZP reference.

	exp^a	CASSCF	XMS-CASPT2	RMS-CASPT2
C_1–C_2	1.408/1.415	1.397	1.405	1.404
C_2–C_6	1.373/1.377	1.386	1.385	1.385
C_6–C_{10}	1.390/1.395	1.388	1.391	1.391
C_{10}–N_{11}	1.460	1.454	1.455	1.454
C_1–N_{14}	1.371	1.392	1.378	1.378
N_{11}–O_{12}	1.246/1.247	1.197	1.240	1.237

^{a} Fig. 3 in Ref. [82]

The solvent effect on geometrical parameters is minimal at the CASSCF level (Table 5; additional parameters can be found in Table S1 in the Supporting Information). The most affected bond is C_{10}–N_{11} (between the nitro group and benzene ring), with a difference of only 0.004 Å between vacuum and water. In contrast, at the CASPT2 level, solvent dependence becomes more pronounced: both C_{10}–N_{11} and C_1–N_{14} bond lengths shorten by 0.013–0.015 Å. The RMS differences between bond lengths in vacuum and water are 1.37×10^{-3}, 7.81×10^{-3}, and 7.07×10^{-3} Å for CASSCF, XMS-CASPT2, and RMS-CASPT2, respectively. This indicates that CASPT2 geometry, incorporating dynamic electron correlation, is more sensitive to solvent polarity.

This difference can be attributed to the larger dipole moment at the CASPT2 level. In vacuum, the dipole moments are 5.311, 6.781, and 6.378 debye at the CASSCF, XMS-CASPT2, and RMS-CASPT2 levels, respectively, indicating a more polarized electronic structure in CASPT2.

Table 5: Solvent dependence of bond lengths C_{10}–N_{11} and C_1–N_{14} (unit in Å) using SA5-CAS(16e,12o)/ANO-RCC-VTZP reference.

| | C_{10}–N_{11} | | | C_1–N_{14} | | |
	CASSCF	XMS[a]	RMS[b]	CASSCF	XMS[a]	RMS[b]
Vacuum	1.454	1.455	1.454	1.392	1.378	1.378
Cyclohexane	1.452	1.455	1.449	1.392	1.374	1.374
Toluene	1.452	1.449	1.448	1.392	1.373	1.374
Dichloroethane	1.451	1.443	1.443	1.391	1.366	1.368
Acetonitrile	1.450	1.441	1.441	1.391	1.365	1.366
Water	1.450	1.440	1.441	1.391	1.363	1.365

[a] XMS-CASPT2
[b] RMS-CASPT2

In water, the dipole moments increase further, to 6.633, 9.071, and 8.460 debye. The greater dipole moments at the CASPT2 levels lead to stronger solvent effects and, consequently, larger changes in the optimized structural parameters. The difference in electronic structures between CASSCF and MS-type CASPT2 can be attributed to two main factors. The first is dynamic electron correlation, arising from electron excitations outside the active space. Although not entirely separable, the second factor involves the rotation of reference and perturbed states (diagonalization of Eqs. (34) and (37)), resulting from rotations within the internal state (CI coefficients). A comparison of the CI coefficients between CASSCF and XMS-CASPT2 for the S_0 state reveals only minor differences, underscoring the importance of dynamic electron correlation.

As presented in Table S1 of the Supporting Information, the reduction in the torsion angle of the amino group[83] is qualitatively reproduced, though the predicted angle is greater than the ADC(2) result. Additionally, crystal packing effects and intermolecular interactions are required to reproduce the experimentally observed planarity of the amino group.

4.3.2 Relaxation of solvent charges

It is advantageous to examine the impact of using the CASPT2 density, comparing the PTE and PTED approaches.[39] As described earlier, geometry optimizations at the CASPT2 level are performed with a fixed reaction field determined at the SCF level (PTE approach). However, single-

point energies can be computed using a more sophisticated method: the reaction field can be determined at the CASPT2 level. The first-order correction to the wavefunction obtained in this way alters the electron density of the solute molecule, and the solvent charges can polarize in response to this perturbed density. Since the wavefunction and solvent charges are non-linearly coupled, the free energy fully coupled with the CASPT2 density is obtained iteratively. This method is referred to as the PTED approach. Although the variational (fully relaxed) density can be obtained during the analytic gradient calculation, the unrelaxed density [excluding the response contribution of the wavefunction at the SCF level ($\overline{\kappa}_{p,q}^{\gamma,[\phi]}$ and $\overline{P}_{\eta,\pi}^{\gamma,[\phi]}$)] is used to compute the PTED energy. Table 6 summarizes the evolution of the equilibrium free energy at both the ground (S_0) and charge-transfer excited states (S_1) in water. The energy at the zeroth iteration corresponds to the PTE energy, while the energy at convergence represents the PTED energy.

Table 6: The free energy $\mathscr{G}_\phi^{[\phi]}$ ($\phi = 0, 1$) (unit in hartree) and the decrease of the energy $\Delta\mathscr{G}_\phi^{[\phi]}$ (unit in eV) in water as a function of the iteration count at (SA5-)XMS-CASPT2(16e,12o)/ANO-RCC-VTZP.

Iteration	$\mathscr{G}_0^{[0]}$	$\Delta\mathscr{G}_0^{[0]}$	$\mathscr{G}_1^{[1]}$	$\Delta\mathscr{G}_1^{[1]}$
1 (PTE)	−491.543 296	—	−491.431 785	—
2	−491.544 107	−0.022	−491.432 834	−0.029
3	−491.544 222	−0.025	−491.432 762	−0.027
4	−491.544 245	−0.026	−491.432 708	−0.025
5	−491.544 252	−0.026	−491.432 684	−0.024
6	−491.544 253	−0.026	−491.432 680	−0.024
7	−491.544 254	−0.026	−491.432 678	−0.024
8 (PTED)	−491.544 255	−0.026	−491.432 678	−0.024

The ground and first excited state energies almost converge by the second iteration. These energies are obtained by performing a CASPT2 calculation with the ASC determined at the SCF level, updating the ASC using the relaxed density, and performing another CASPT2 calculation with the updated ASC. Unlike single-reference methods, a significant part of the density is determined by the zeroth-order wavefunction for both the initial and final states, while the first-order correction from the PT2 calculation is perturbative. Consequently, relaxation has a minimal impact. The

31

first cycle yields an energy decrease of 0.02 eV and 0.03 eV for the S_0 and S_1 states, respectively, indicating that full relaxation is not critical. Furthermore, the difference in equilibrium energies between the PTE (3.034 eV) and PTED (3.036 eV) approaches is only 0.002 eV ($\approx$ 0.5 kcal mol^{-1}), suggesting that, in practice, the relaxation correction for transition energies is below the expected accuracy of the MRPT method. For this specific case, the PTE approach accurately reproduces the PTED energy difference, and thus, PTE energies are used hereafter. It is important to note that these energies represent equilibrium energies and are not directly applicable to absorption energy calculations, which require a non-equilibrium solvation model.

A similar comparison, using the relaxed density matrix to compute the analytic gradient including $\overline{\kappa}_{p,q}^{\gamma,[\phi]}$ and $\overline{P}_{\eta,\pi}^{\gamma,[\phi]}$ is provided in the Supporting Information (Table S2). This result follows the same trend as that observed with the unrelaxed density: the difference between the PTE and PTED approaches is small but slightly larger (0.005 eV $\approx$ 1 kcal mol^{-1}) when using the relaxed density. Nevertheless, in both cases, the difference is relatively minor and may only be non-negligible if extremely high accuracy is required or if the difference of interest is particularly small (e.g., the singlet–triplet gap).[59]

4.3.3 Absorption energies

Finally, absorption energies for the transition from the closed-shell ground state to the lowest charge-transfer state were calculated using CASSCF, XMS-CASPT2, and RMS-CASPT2, and are summarized in Table 7. These energies were computed using a non-equilibrium solvation model. First, the reaction field is generated at the closed-shell ground state with dielectric constant ε. The slow component is fixed with this reaction field, while the fast component is determined at the charge-transfer excited state using ε^∞. The non-equilibrium energy for acetonitrile and water at the CASSCF level could not be obtained due to the quasi-degeneracy of the target state during SCF, so absorption energies were computed using nearly converged energy for reference (after 200 SCF iterations). A potential solution involves mixing density matrices of nearby states, but the oscillator strength of the transition from S_0 to any excited states other than the target charge-transfer state is

32

smaller by two to three orders of magnitude (as shown by state interaction calculations[84]), making this approach difficult to validate. Furthermore, since the ordering of states at the SCF and PT2 levels can be different, averaging other states at the SCF level does not necessarily correspond to averaging them at the PT2 level.

Table 7: Absorption energies (unit in eV) to the charge-transfer state with the SA5-CAS(16e,12o)/ANO-RCC-VTZP reference.

Solvent	ε	ε_∞	Exp.	CASSCF	XMS-CASPT2	RMS-CASPT2
Vacuum	—	—	4.24^a	6.227	3.969	4.024
Cyclohexane	2.023	2.028	3.84^b	5.802	3.579	3.695
Toluene	2.379	2.232	3.60^c	5.733	3.402	3.492
Dichloroethane	10.36	2.085		5.575	3.277	3.319
Acetonitrile	36.64	1.806	3.41^b	$(5.591)^d$	3.288	3.373
Water (PCM)	78.39	1.776	3.25^b	$(5.593)^d$	3.286	3.373
Water (PCM + 2H$_2$O)	78.39	1.776	3.25^b	$—^e$	2.978	3.134

^{a} Ref. 85 ^{b} Ref. 86 ^{c} Ref. 87 ^{d} Non-equilibrium calculation at the excited state did not fully converge. ^{e} Geometry optimization did not converge.

CASSCF calculations significantly overestimated the absorption energies. In contrast, both CASPT2 methods underestimated these energies by 0.1–0.3 eV, as is commonly known. The IPEA shift technique,[69] designed to address this issue, resulted in overestimated absorption energies (e.g., 4.569 eV with XMS-CASPT2 in vacuum when using the recommended IPEA shift of 0.25). Therefore, only results without the IPEA shift are presented. The deviation is still close to the expected accuracy of CASPT2.

Experimentally, the solvatochromic shift in water is approximately 1 eV, but this shift was underestimated by CASPT2 calculations with PCM without explicit solvent molecules. Even though XMS-CASPT2 with PCM could reproduce the experimental absorption energy in water very well, this fortuitous agreement is mostly attributed to the error cancellation. Since the description of solvent with PCM is rather limited, adding a few explicit solvent molecules can be effective. While the combination of implicit and explicit solvation models is a typical approach to remedy the poor treatment of the local solute–solvent interaction in PCM, it should be noted that explicit solvation

33

approaches have limitations: the number and positions of solvent molecules are rather arbitrary, they may overestimate solute–solvent interactions,[88] and parameters used in PCM are typically optimized without considering the presence of explicit molecules. Still, if two water molecules are explicit included in addition to PCM, we observe an additional shift of more than 0.2 eV, and the solvatochromic shift of water is approximately 1 eV with CASPT2, being consistent with experiment. Geometry optimization at the CASSCF level with two explicit water molecules did not converge, because of the lack of the dynamical electron correlation (dispersion).

5 Conclusions

The analytic gradient and NAC vectors for SA-MCSCF and CASPT2 with PCM have been derived and implemented in a development version of the open-source package OpenMolcas. The current formulation of the energy, which has been in use in (Open)Molcas, relies on the state-averaged solute energy with a state-specific solvation model (Eq. (15)) for SA-MCSCF. For regions of state crossings, the solvent charges are polarized with respect to the averaged density of the crossing states, ensuring that the PESs near the crossing region remain smooth, as illustrated in Figures 1 and 2. As discussed, an approximate electronic gradient is employed to solve the SCF equation. However, analytic derivatives can be obtained by using the exact gradient of the approximate electronic gradient and solving a modified Z-vector equation with internal state rotations. We observed that fully relaxing the solvent charge with the CASPT2 density had a negligible effect on the excitation energy, indicating that the PTE approach is sufficient for CASPT2 with PCM. The experimental solvatochromic shift could also be reproduced using this method and explicit solvent molecules.

While PCM is useful, it cannot explicitly describe the solvent structure and thermal fluctuations, leading to inaccuracies in modeling intermolecular interactions. This is clearly demonstrated by the calculation with explicit solvent molecules (Table 7). To address this, the RISM method or the recently developed fluctuating charge force field,[89] available in OpenMolcas, could

34

prove beneficial. Furthermore, the current formulation does not yield the variational minimum of the state-averaged energy. Given these limitations, it would be worth exploring the possibility of integrating the recent formulation for RISM.[90] Additionally, the present method cannot be applied to molecular dynamics simulations that involve non-adiabatic transitions, as it assumes the solvent is polarized with respect to a specific density. A preliminary implementation of a dynamic solvation model, including analytic derivatives, seems promising and could be a potential direction for future work. We plan to formally release the developed code as a part of OpenMolcas in the near future.

Acknowledgement

Supporting Information Available

The Supporting Information is available free of charge at...

Active space of *para*-nitroaniline, PESs of acrolein, geometrical parameters of *para*-nitroaniline, effect of the relaxed charge, and optimized coordinates.

Appendix

Following Refs. 43 and 91, the wavefunction is parametrized as:

$$|\check{\Psi}_\gamma^{(0)}\rangle = \exp(-\hat{\kappa})\exp(-\hat{P}_\gamma)|\Psi_\gamma^{(0)}\rangle \tag{45}$$

where $\hat{\kappa}$ is the orbital rotation operator

$$\hat{\kappa} = \sum_{p>q} \kappa_{p,q} \hat{E}_{p,q}^- = \sum_{p>q} \kappa_{p,q} (\hat{E}_{p,q} - \hat{E}_{q,p}) \tag{46}$$

and $\hat{P}_\gamma$ is the state transfer operator

$$\hat{P}_\gamma = \sum_{\gamma>\pi} P_{\gamma,\pi} (|\gamma\rangle\langle\pi| - |\pi\rangle\langle\gamma|) \tag{47}$$

In the conventional SA-MCSCF case,[91,92] the state transfer parameter can be entirely projected onto the CSF space. However, for SA-MCSCF/PCM, the energy is not generally invariant with respect to rotations between internal states, requiring the consideration of additional parameters. In practice, rotations between internal and external states are projected onto the CSF space, while rotations between internal states are handled separately. For simplicity, the zeroth-order wavefunction is denoted by the state index: $|\gamma\rangle = |\Psi_\gamma^{(0)}\rangle$.

The gradient of the state-averaged energy (Eq. (15)) with respect to the wavefunction parameters is obtained by taking partial derivatives with respect to the rotation parameters $\kappa_{p,q}$ and $P_{\gamma,\pi}$. The analytic orbital gradient is expressed as:

$$\frac{\partial \mathscr{E}_{\text{SA}}^{[\phi]}}{\partial \kappa_{p,q}} = \sum_{\gamma\in\mathscr{P}} \omega_\gamma \left\langle \gamma \left| \left[\hat{E}_{p,q}^-, \hat{H}^{\text{vac}} + \hat{V}^{[\phi]} \right] \right| \gamma \right\rangle - \sum_i \sum_{r,s} \left\langle \phi \left| [\hat{E}_{p,q}^-, \hat{E}_{r,s}] \right| \phi \right\rangle \left\langle r \left| \frac{Q_i^{\text{e,SA}} - Q_i^{\text{e},[\phi]}}{|\mathbf{r} - \mathbf{r}_i|} \right| s \right\rangle \tag{48}$$

and the CI gradient is given by:

$$\frac{\partial \mathscr{E}_{\text{SA}}^{[\phi]}}{\partial P_{\eta,\pi}} = 2 \left(\omega_\eta - \sum_{\gamma\in\mathscr{P}} \omega_\gamma \delta_{\gamma\pi} \right) \left\langle \eta \left| \hat{H}^{\text{vac}} + \hat{V}^{[\phi]} \right| \pi \right\rangle$$
$$- 2 \left(\delta_{\phi,\eta} - \delta_{\phi,\pi} \right) \sum_i \sum_{p,q} \left\langle \eta \left| \hat{E}_{p,q} \right| \pi \right\rangle \left\langle p \left| \frac{Q_i^{\text{e,SA}} - Q_i^{\text{e},[\phi]}}{|\mathbf{r} - \mathbf{r}_i|} \right| q \right\rangle . \tag{49}$$

As discussed in the main text, the approximate gradient used in the actual calculations is obtained

by neglecting the second term:

$$\frac{\partial \mathscr{E}_{\text{SA}}^{[\phi]}}{\partial \kappa_{p,q}} \approx \sum_{\gamma \in \mathscr{P}} \omega_{\gamma} \left\langle \gamma \left| \left[\hat{E}_{p,q}^-, \hat{H}^{\text{vac}} + \hat{V}^{[\phi]} \right] \right| \gamma \right\rangle =: \frac{\partial \widetilde{\mathscr{E}}_{\text{SA}}^{[\phi]}}{\partial \kappa_{p,q}} ,\tag{50}$$

$$\frac{\partial \mathscr{E}_{\text{SA}}^{[\phi]}}{\partial P_{\eta,\pi}} \approx 2 \left(\omega_{\eta} - \sum_{\gamma \in \mathscr{P}} \omega_{\gamma} \delta_{\gamma \pi} \right) \left\langle \eta \left| \hat{H}^{\text{vac}} + \hat{V}^{[\phi]} \right| \pi \right\rangle =: \frac{\partial \widetilde{\mathscr{E}}_{\text{SA}}^{[\phi]}}{\partial P_{\eta,\pi}}\tag{51}$$

The approximate gradient is thus defined by $(\partial \widetilde{\mathscr{E}}_{\text{SA}}^{[\phi]})/(\partial \kappa_{p,q})$ and $(\partial \widetilde{\mathscr{E}}_{\text{SA}}^{[\phi]})/(\partial P_{\eta,\pi})$. No analytic expression exists for $\widetilde{\mathscr{E}}_{\text{SA}}^{[\phi]}$. The neglected term implies that we can variationally minimize the state-averaged energy without further modification if the solvent reaction field is generated using the state-averaged density ($\mathbf{Q}^{\text{e},[\phi]} \to \mathbf{Q}^{\text{e,SA}}$) or if SS-MCSCF ($\mathbf{Q}^{\text{e,SA}} \to \mathbf{Q}^{\text{e},[\phi]}$) is employed. However, these introduces other challenges discussed in the main text. The approximation worsens as the number of averaged states increases, making it preferable, in principle, to restrict the number of states being averaged. However, this introduces challenges similar to the root-flipping problem.

The rotation Hessian employed in this study can be obtained by taking a derivative of $\widetilde{\mathscr{E}}_{\text{SA}}^{[\phi]}$ (but not $\mathscr{E}_{\text{SA}}^{[\phi]}$) twice. The orbital–orbital rotation Hessian is given by:

$$\begin{aligned}
\frac{\partial^2 \widetilde{\mathscr{E}}_{\text{SA}}^{[\phi]}}{\partial \kappa_{p,q} \partial \kappa_{r,s}} &= \frac{\partial}{\partial \kappa_{p,q}} \frac{\partial \widetilde{\mathscr{E}}_{\text{SA}}^{[\phi]}}{\partial \kappa_{r,s}} \\
&= \sum_{\gamma \in \mathscr{P}} \omega_{\gamma} \left\langle \gamma \left| \left[\hat{E}_{p,q}^-, \left[\hat{E}_{r,s}^-, \hat{H}^{\text{vac}} + \hat{V}^{[\phi]} \right] \right] \right| \gamma \right\rangle \\
&\quad - \sum_{t,u} \sum_i \left\langle \phi \left| \left[\hat{E}_{p,q}^-, \hat{E}_{t,u} \right] \right| \phi \right\rangle \left\langle t \left| \frac{\mathscr{Q}_{r,s}^{\text{e,SA}}(i)}{|\mathbf{r} - \mathbf{r}_i|} \right| u \right\rangle ,
\end{aligned}\tag{52}$$

where

$$\begin{aligned}
\mathscr{Q}_{r,s}^{\text{e,SA}}(i) &= -\frac{\varepsilon - 1}{\varepsilon} \sum_j \left(\mathbf{C}^{-1} \right)_{i,j} \mathscr{V}_{r,s}^{\text{e,SA}}(j) \\
&= \frac{\varepsilon - 1}{\varepsilon} \sum_j \left(\mathbf{C}^{-1} \right)_{i,j} \sum_{\gamma \in \mathscr{P}} \omega_{\gamma} \sum_{p,q} \left\langle \gamma \left| \left[\hat{E}_{r,s}^-, \hat{E}_{p,q} \right] \right| \gamma \right\rangle \left\langle p \left| \frac{1}{|\mathbf{r} - \mathbf{r}_j|} \right| q \right\rangle .
\end{aligned}\tag{53}$$

The first term in Eq. (52) can be made symmetric, whereas the second term, newly added for PCM,

37

is not symmetric ($\hat{E}_{p,q}$ operates on the ϕth state only, whereas $\hat{E}_{r,s}$ operators on the averaged state).

The CI–orbital rotation Hessian is

$$
\begin{aligned}
\frac{\partial^2 \widetilde{\mathscr{E}}_{\mathrm{SA}}^{[\phi]}}{\partial P_{\eta,\pi} \partial \kappa_{p,q}} &= \frac{\partial}{\partial P_{\eta,\pi}} \frac{\partial \widetilde{\mathscr{E}}_{\mathrm{SA}}^{[\phi]}}{\partial \kappa_{p,q}} \\
&= 2 \left(\omega_\eta - \sum_{\gamma \in \mathscr{P}} \omega_\gamma \delta_{\gamma\pi} \right) \left\langle \eta \left| \left[\hat{E}_{p,q}^-, \hat{H}^{\mathrm{vac}} + \hat{V}^{[\phi]} \right] \right| \pi \right\rangle \\
&\quad - 2 \left(\delta_{\phi,\eta} - \delta_{\phi,\pi} \right) \sum_i \sum_{r,s} \left\langle \eta \left| \hat{E}_{r,s} \right| \pi \right\rangle \left\langle r \left| \frac{\mathscr{Q}_{p,q}^{\mathrm{e,SA}}(i)}{|\mathbf{r} - \mathbf{r}_i|} \right| s \right\rangle .
\end{aligned}
\tag{54}
$$

The orbital–CI rotation Hessian is

$$
\begin{aligned}
\frac{\partial^2 \widetilde{\mathscr{E}}_{\mathrm{SA}}^{[\phi]}}{\partial \kappa_{p,q} \partial P_{\eta,\pi}} &= \frac{\partial}{\partial \kappa_{p,q}} \frac{\partial \widetilde{\mathscr{E}}_{\mathrm{SA}}^{[\phi]}}{\partial P_{\eta,\pi}} \\
&= 2 \left(\omega_\eta - \sum_{\gamma \in \mathscr{P}} \omega_\gamma \delta_{\gamma,\pi} \right) \left\langle \eta \left| \left[\hat{E}_{p,q}^-, \hat{H}^{\mathrm{vac}} + \hat{V}^{[\phi]} \right] \right| \pi \right\rangle \\
&\quad - 2 \sum_{r,s} \sum_i \left\langle \phi \left| \left[\hat{E}_{p,q}^-, \hat{E}_{r,s} \right] \right| \phi \right\rangle \left\langle r \left| \frac{\mathscr{Q}_{\eta,\pi}(i)}{|\mathbf{r} - \mathbf{r}_i|} \right| s \right\rangle ,
\end{aligned}
\tag{55}
$$

where

$$
\mathscr{Q}_{\eta,\pi}(i) = \frac{\varepsilon - 1}{\varepsilon} \sum_j \left(\mathbf{C}^{-1} \right)_{i,j} \left(\omega_\eta - \sum_{\gamma \in \mathscr{P}} \omega_\gamma \delta_{\gamma,\pi} \right) \sum_{p,q} \left\langle \eta \left| \hat{E}_{p,q} \right| \pi \right\rangle \left\langle p \left| \frac{1}{|\mathbf{r} - \mathbf{r}_j|} \right| q \right\rangle .
\tag{56}
$$

The CI–CI rotation Hessian is

$$
\begin{aligned}
\frac{\partial^2 \widetilde{\mathscr{E}}_{\mathrm{SA}}^{[\phi]}}{\partial P_{\eta,\pi} \partial P_{\theta,\rho}} &= \frac{\partial}{\partial P_{\eta,\pi}} \frac{\partial \widetilde{\mathscr{E}}_{\mathrm{SA}}^{[\phi]}}{\partial P_{\theta,\rho}} \\
&= 2 \left(\omega_\eta - \sum_{\gamma \in \mathscr{P}} \omega_\gamma \delta_{\gamma,\pi} \right) \left(1 - \hat{\tau}_{\theta,\rho} \right) \left(1 + \hat{\tau}_{\eta,\pi} \right) \delta_{\eta,\theta} \left\langle \pi \left| \hat{H} + \hat{V}^{[\phi]} \right| \rho \right\rangle \\
&\quad - 2 \left(\delta_{\phi,\eta} - \delta_{\phi,\pi} \right) \sum_{p,q} \sum_i \left\langle \eta \left| \hat{E}_{p,q} \right| \pi \right\rangle \left\langle p \left| \frac{\mathscr{Q}_{\theta,\rho}(i)}{|\mathbf{r} - \mathbf{r}_i|} \right| q \right\rangle ,
\end{aligned}
\tag{57}
$$

where $\hat{\tau}_{p,q}$ permutes the indices p and q.

38

References

(1) Musiał, M.; Perera, A.; Bartlett, R. J. Multireference Coupled-Cluster Theory: The Easy Way. *J. Chem. Phys.* **2011**, *134*, 114108.

(2) Lyakh, D. I.; Musiał, M.; Lotrich, V. F.; Bartlett, R. J. Multireference Nature of Chemistry: The Coupled-Cluster View. *Chem. Rev.* **2012**, *112*, 182–243.

(3) Köhn, A.; Hanauer, M.; Mück, L. A.; Jagau, T.-C.; Gauss, J. State-Specific Multireference Coupled-Cluster Theory. *WIREs Comput. Mol. Sci.* **2013**, *3*, 176–197.

(4) Szalay, P. G.; Müller, T.; Gidofalvi, G.; Lischka, H.; Shepard, R. Multiconfiguration Self-Consistent Field and Multireference Configuration Interaction Methods and Applications. *Chem. Rev.* **2012**, *112*, 108–181.

(5) Roos, B. O.; Linse, P.; Siegbahn, P. E. M.; Blomberg, M. R. A. A Simple Method for the Evaluation of the Second-Order-Perturbation Energy from External Double-Excitations with a CASSCF Reference Wavefunction. *Chem. Phys.* **1982**, *66*, 197 – 207.

(6) Andersson, K.; Malmqvist, P.-Å.; Roos, B. O.; Sadlej, A. J.; Wolinski, K. Second-Order Perturbation Theory with a CASSCF Reference Function. *J. Phys. Chem.* **1990**, *94*, 5483–5488.

(7) Andersson, K.; Malmqvist, P.-Å.; Roos, B. O. Second-Order Perturbation Theory with a Complete Active Space Self-Consistent Field Reference Function. *J. Chem. Phys.* **1992**, *96*, 1218–1226.

(8) Šulka, M.; Šulková, K.; Jurečka, P.; Dubecký, M. Dynamic and Nondynamic Electron Correlation Energy Decomposition Based on the Node of the Hartree–Fock Slater Determinant. *J. Chem. Theory Comput.* **2023**, *19*, 8147–8155.

(9) Šulka, M.; Šulková, K.; Dubecký, M. Unveiling hidden dynamic correlations in CASSCF correlation energies by Hartree–Fock nodes. *J. Chem. Phys.* **2024**, *161*, 114112.

(10) Izsák, R. Single-reference coupled cluster methods for computing excitation energies in large molecules: The efficiency and accuracy of approximations. *WIREs Comput. Mol. Sci.* **2020**, *10*, e1445.

(11) Lin, H.; Truhlar, D. G. QM/MM: What Have We Learned, Where Are We, and Where Do We Go from Here? *Theor. Chem. Acc.* **2007**, *117*, 185–199.

(12) Kosugi, T.; Hayashi, S. QM/MM Reweighting Free Energy SCF for Geometry Optimization on Extensive Free Energy Surface of Enzymatic Reaction. *J. Chem. Theory Comput.* **2012**, *8*, 322–334.

(13) Gordon, M. S.; Freitag, M. A.; Bandyopadhyay, P.; Jensen, J. H.; Kairys, V.; Stevens, W. J. The Effective Fragment Potential Method: A QM-Based MM Approach to Modeling Environmental Effects in Chemistry. *J. Phys. Chem. A* **2001**, *105*, 293–307.

(14) Gordon, M. S.; Smith, Q. A.; Xu, P.; Slipchenko, L. V. Accurate First Principles Model Potentials for Intermolecular Interactions. *Annu. Rev. Phys. Chem.* **2013**, *64*, 553–578.

(15) Still, W. C.; Tempczyk, A.; Hawley, R. C.; Hendrickson, T. Semianalytical Treatment of Solvation for Molecular Mechanics and Dynamics. *J. Am. Chem. Soc.* **1990**, *112*, 6127–6129.

(16) Qiu, D.; Shenkin, P. S.; Hollinger, F. P.; Still, W. C. The GB/SA Continuum Model for Solvation. A Fast Analytical Method for the Calculation of Approximate Born Radii. *J. Phys. Chem. A* **1997**, *101*, 3005–3014.

(17) Tomasi, J.; Mennucci, B.; Cammi, R. Quantum Mechanical Continuum Solvation Models. *Chem. Rev.* **2005**, *105*, 2999–3094.

(18) Klamt, A.; Schüürmann, G. COSMO: A New Approach to Dielectric Screening in Solvents with Explicit Expressions for the Screening Energy and Its Gradient. *J. Chem. Soc., Perkin Trans. 2* **1993**, 799–805.

(19) Ten-no, S.; Hirata, F.; Kato, S. A Hybrid Approach for the Solvent Effect on the Electronic Structure of a Solute Based on the RISM and Hartree-Fock Equations. *Chem. Phys. Lett.* **1993**, *214*, 391–396.

(20) Sato, H.; Hirata, F.; Kato, S. Analytical Energy Gradient for the Reference Interaction Site Model Multiconfigurational Self-Consistent-Field Method: Application to 1,2-Difluoroethylene in Aqueous Solution. *J. Chem. Phys.* **1996**, *105*, 1546–1551.

(21) Amovilli, C.; Mennucci, B.; Floris, F. M. MCSCF Study of the S_N2 Menshutkin Reaction in Aqueous Solution within the Polarizable Continuum Model. *J. Phys. Chem. B* **1998**, *102*, 3023–3028.

(22) Mennucci, B.; Cammi, R.; Tomasi, J. Excited States and Solvatochromic Shifts within a Nonequilibrium Solvation Approach: A New Formulation of the Integral Equation Formalism Method at the Self-Consistent Field, Configuration Interaction, and Multiconfiguration Self-Consistent Field Level. *J. Chem. Phys.* **1998**, *109*, 2798–2807.

(23) Cammi, R.; Mennucci, B.; Tomasi, J. Second-Order Møller-Plesset Analytical Derivatives for the Polarizable Continuum Model Using the Relaxed Density Approach. *J. Phys. Chem. A* **1999**, *103*, 9100–9108.

(24) Cammi, R. Quantum Cluster Theory for the Polarizable Continuum Model. I. The CCSD Level with Analytical First and Second Derivatives. *J. Chem. Phys.* **2009**, *131*, 164104.

(25) Cammi, R. Coupled-cluster theories for the polarizable continuum model. II. Analytical gradients for excited states of molecular solutes by the equation of motion coupled-cluster method. *Int. J. Quantum Chem.* **2010**, *110*, 3040–3052.

(26) Cammi, R.; Fukuda, R.; Ehara, M.; Nakatsuji, H. Symmetry-adapted cluster and symmetry-adapted cluster-configuration interaction method in the polarizable continuum model: Theory of the solvent effect on the electronic excitation of molecules in solution. *J. Chem. Phys.* **2010**, *133*, 024104.

41

(27) Song, C. State-averaged CASSCF with polarizable continuum model for studying photore-actions in solvents: Energies, analytical nuclear gradients, and non-adiabatic couplings. *J. Chem. Phys.* **2022**, *156*, 104102.

(28) Liu, X.; Humeniuk, A.; Glover, W. J. Conical Intersections in Solution with Polarizable Embedding: Integral-Exact Direct Reaction Field. *J. Chem. Theory Comput.* **2022**, *18*, 6826–6839.

(29) Song, C. State averaged CASSCF in AMOEBA polarizable water model for simulating nonadiabatic molecular dynamics with nonequilibrium solvation effects. *J. Chem. Phys.* **2023**, *158*, 014101.

(30) Humeniuk, A.; Glover, W. J. Multistate, Polarizable QM/MM Embedding Scheme Based on the Direct Reaction Field Method: Solvatochromic Shifts, Analytical Gradients and Optimizations of Conical Intersections in Solution. *J. Chem. Theory Comput.* **2024**, *20*, 2111–2126.

(31) Yamazaki, S.; Kato, S. Locating the lowest free-energy point on conical intersection in polar solvent: Reference interaction site model self-consistent field study of ethylene and CH2NH2+. *J. Chem. Phys.* **2005**, *123*, 114510.

(32) Mori, T.; Nakano, K.; Kato, S. Conical Intersections of Free Energy Surfaces in Solution: Effect of Electron Correlation on a Protonated Schiff Base in Methanol Solution. *J. Chem. Phys.* **2010**, *133*, 064107.

(33) Park, J. W.; Shiozaki, T. On-the-Fly CASPT2 Surface-Hopping Dynamics. *J. Chem. Theory Comput.* **2017**, *13*, 3676–3683.

(34) Bezabih, M. S.; Kaliakin, D. S.; Blanco-González, A.; Barneschi, L.; Tarnovsky, A. N.; Olivucci, M. Comparative Study of Uracil Excited-State Photophysics in Water and Acetonitrile via RMS-CASPT2-Driven Quantum-Classical Trajectories. *J. Phys. Chem. B* **2023**, *127*, 10871–10879.

(35) Hagras, M. A.; Glover, W. J. Polarizable Embedding for Excited-State Reactions: Dynamically Weighted Polarizable QM/MM. *J. Chem. Theory Comput.* **2018**, *14*, 2137–2144.

(36) Fdez. Galván, I.; Vacher, M.; Alavi, A.; Angeli, C.; Aquilante, F.; Autschbach, J.; Bao, J. J.; Bokarev, S. I.; Bogdanov, N. A.; Carlson, R. K.; Chibotaru, L. F.; Creutzberg, J.; Dattani, N.; Delcey, M. G.; Dong, S. S.; Dreuw, A.; Freitag, L.; Frutos, L. M.; Gagliardi, L.; Gendron, F.; Giussani, A.; González, L.; Grell, G.; Guo, M.; Hoyer, C. E.; Johansson, M.; Keller, S.; Knecht, S.; Kovačević, G.; Källman, E.; Li Manni, G.; Lundberg, M.; Ma, Y.; Mai, S.; Malhado, J. P.; Malmqvist, P.-Å.; Marquetand, P.; Mewes, S. A.; Norell, J.; Olivucci, M.; Oppel, M.; Phung, Q. M.; Pierloot, K.; Plasser, F.; Reiher, M.; Sand, A. M.; Schapiro, I.; Sharma, P.; Stein, C. J.; Sørensen, L. K.; Truhlar, D. G.; Ugandi, M.; Ungur, L.; Valentini, A.; Vancoillie, S.; Veryazov, V.; Weser, O.; Wesołowski, T. A.; Widmark, P.-O.; Wouters, S.; Zech, A.; Zobel, J. P.; Lindh, R. OpenMolcas: From Source Code to Insight. *J. Chem. Theory Comput.* **2019**, *15*, 5925–5964.

(37) Aquilante, F.; Autschbach, J.; Baiardi, A.; Battaglia, S.; Borin, V. A.; Chibotaru, L. F.; Conti, I.; De Vico, L.; Delcey, M.; Fdez. Galván, I.; Ferré, N.; Freitag, L.; Garavelli, M.; Gong, X.; Knecht, S.; Larsson, E. D.; Lindh, R.; Lundberg, M.; Malmqvist, P. Å.; Nenov, A.; Norell, J.; Odelius, M.; Olivucci, M.; Pedersen, T. B.; Pedraza-González, L.; Phung, Q. M.; Pierloot, K.; Reiher, M.; Schapiro, I.; Segarra-Martí, J.; Segatta, F.; Seijo, L.; Sen, S.; Sergentu, D.-C.; Stein, C. J.; Ungur, L.; Vacher, M.; Valentini, A.; Veryazov, V. Modern quantum chemistry with [Open]Molcas. *J. Chem. Phys.* **2020**, *152*, 214117.

(38) Li Manni, G.; Fdez. Galván, I.; Alavi, A.; Aleotti, F.; Aquilante, F.; Autschbach, J.; Avagliano, D.; Baiardi, A.; Bao, J. J.; Battaglia, S.; Birnoschi, L.; Blanco-González, A.; Bokarev, S. I.; Broer, R.; Cacciari, R.; Calio, P. B.; Carlson, R. K.; Carvalho Couto, R.; Cerdán, L.; Chibotaru, L. F.; Chilton, N. F.; Church, J. R.; Conti, I.; Coriani, S.; Cuéllar-Zuquin, J.; Daoud, R. E.; Dattani, N.; Decleva, P.; de Graaf, C.; Delcey, M. G.; De Vico, L.; Dobrautz, W.; Dong, S. S.; Feng, R.; Ferré, N.; Filatov(Gulak), M.; Gagliardi, L.; Gar-

avelli, M.; González, L.; Guan, Y.; Guo, M.; Hennefarth, M. R.; Hermes, M. R.; Hoyer, C. E.; Huix-Rotllant, M.; Jaiswal, V. K.; Kaiser, A.; Kaliakin, D. S.; Khamesian, M.; King, D. S.; Kochetov, V.; Krośnicki, M.; Kumaar, A. A.; Larsson, E. D.; Lehtola, S.; Lepetit, M.-B.; Lischka, H.; López Ríos, P.; Lundberg, M.; Ma, D.; Mai, S.; Marquetand, P.; Merritt, I. C. D.; Montorsi, F.; Mörchen, M.; Nenov, A.; Nguyen, V. H. A.; Nishimoto, Y.; Oakley, M. S.; Olivucci, M.; Oppel, M.; Padula, D.; Pandharkar, R.; Phung, Q. M.; Plasser, F.; Raggi, G.; Rebolini, E.; Reiher, M.; Rivalta, I.; Roca-Sanjuán, D.; Romig, T.; Safari, A. A.; Sánchez-Mansilla, A.; Sand, A. M.; Schapiro, I.; Scott, T. R.; Segarra-Martí, J.; Segatta, F.; Sergentu, D.-C.; Sharma, P.; Shepard, R.; Shu, Y.; Staab, J. K.; Straatsma, T. P.; Sørensen, L. K.; Tenorio, B. N. C.; Truhlar, D. G.; Ungur, L.; Vacher, M.; Veryazov, V.; Voß, T. A.; Weser, O.; Wu, D.; Yang, X.; Yarkony, D.; Zhou, C.; Zobel, J. P.; Lindh, R. The OpenMolcas Web: A Community-Driven Approach to Advancing Computational Chemistry. *J. Chem. Theory Comput.* **2023**, *19*, 6933–6991.

(39) del Valle, F.; Tomasi, J. Electron correlation and solvation effects. I. Basic formulation and preliminary attempt to include the electron correlation in the quantum mechanical polarizable continuum model so as to study solvation phenomena. *Chem. Phys.* **1991**, *150*, 139–150.

(40) Malmqvist, P.-Å.; Rendell, A.; Roos, B. O. The Restricted Active Space Self-Consistent-Field Method, Implemented with a Split Graph Unitary Group Approach. *J. Phys. Chem.* **1990**, *94*, 5477–5482.

(41) Celani, P.; Werner, H.-J. Multireference Perturbation Theory for Large Restricted and Selected Active Space Reference Wave Functions. *J. Chem. Phys.* **2000**, *112*, 5546–5557.

(42) Malmqvist, P.-Å.; Pierloot, K.; Shahi, A. R. M.; Cramer, C. J.; Gagliardi, L. The Restricted Active Space Followed by Second-Order Perturbation Theory Method: Theory and Application to the Study of CuO_2 and Cu_2O_2 Systems. *J. Chem. Phys.* **2008**, *128*, 204109.

(43) Helgaker, T., Jørgensen, P., Olsen, J., Eds. *Molecular Electronic-Structure Theory*; John Wiley & Sons, Ltd.: England, 2000.

(44) Tran, L. N.; Shea, J. A. R.; Neuscamman, E. Tracking Excited States in Wave Function Optimization Using Density Matrices and Variational Principles. *J. Chem. Theory Comput.* **2019**, *15*, 4790–4803.

(45) Bernhardsson, A.; Lindh, R.; Karlström, G.; Roos, B. O. Direct self-consistent reaction field with Pauli repulsion: solvation effects on methylene peroxide. *Chem. Phys. Lett.* **1996**, *251*, 141–149.

(46) Serrano-Andrés, L.; Fülscher, M. P.; Karlström, G. Solvent effects on electronic spectra studied by multiconfigurational perturbation theory. *Int. J. Quantum Chem.* **1997**, *65*, 167–181.

(47) Proppe, B.; Merchán, M.; Serrano-Andrés, L. Theoretical Study of the Twisted Intramolecular Charge Transfer in 1-Phenylpyrrole. *J. Phys. Chem. A* **2000**, *104*, 1608–1616.

(48) Cui, G.; Cao, X.-Y.; Fang, W.-H.; Dolg, M.; Thiel, W. Photoinduced Gold(I)–Gold(I) Chemical Bonding in Dicyanoaurate Oligomers. *Angew. Chem. Int. Ed.* **2013**, *52*, 10281–10285.

(49) Xiao, P.; Li, C.-X.; Fang, W.-H.; Cui, G.; Thiel, W. Mechanism of the Visible-Light-Mediated Copper-Catalyzed Coupling Reaction of Phenols and Alkynes. *J. Am. Chem. Soc.* **2018**, *140*, 15099–15113.

(50) Fang, Y.-G.; Valverde, D.; Mai, S.; Canuto, S.; Borin, A. C.; Cui, G.; González, L. Excited-State Properties and Relaxation Pathways of Selenium-Substituted Guanine Nucleobase in Aqueous Solution and DNA Duplex. *J. Phys. Chem. B* **2021**, *125*, 1778–1789.

(51) González Moreno, A.; de Cózar, A.; Prieto, P.; Domínguez, E.; Heredia, A. Radiationless mechanism of UV deactivation by cuticle phenolics in plants. *Nat. Commun.* **2022**, *13*, 1786.

(52) Soto, J.; Peláez, D.; Algarra, M. CASPT2 study of the electronic structure and photochemistry of protonated N-nitrosodimethylamine (NDMA-H+) at 453 nm. *The Journal of Chemical Physics* **2023**, *158*, 204301.

(53) Shimizu, R. Y.; Yanai, T.; Yokogawa, D. Improved RISM-CASSCF Optimization via State-Average Treatment and Damping for Characterizing Excited Molecules in Solution with Multireference Perturbation Theory. *J. Chem. Theory Comput.* **2020**, *16*, 4865–4873.

(54) Sonneveld, P. CGS, A Fast Lanczos-Type Solver for Nonsymmetric Linear systems. *SIAM J. Sci. Stat. Comput.* **1989**, *10*, 36–52.

(55) Itoh, S.; Sugihara, M. Preconditioned Algorithm of the CGS Method Focusing on Its Deriving Process (Japanese literature). *Trans. Jpn. Soc. Ind. Appl. Math.* **2013**, *23*, 253–286.

(56) Fdez. Galván, I.; Delcey, M. G.; Pedersen, T. B.; Aquilante, F.; Lindh, R. Analytical State-Average Complete-Active-Space Self-Consistent Field Nonadiabatic Coupling Vectors: Implementation with Density-Fitted Two-Electron Integrals and Application to Conical Intersections. *J. Chem. Theory Comput.* **2016**, *12*, 3636–3653.

(57) Barone, V.; Cossi, M. Quantum Calculation of Molecular Energies and Energy Gradients in Solution by a Conductor Solvent Model. *J. Phys. Chem. A* **1998**, *102*, 1995–2001.

(58) Riccardo Spezia, I. B.; Hynes, J. T. Conical intersections in solution: non-equilibrium versus equilibrium solvation. *Mol. Phys.* **2006**, *104*, 903–914.

(59) Saitow, M.; Hori, K.; Yoshikawa, A.; Shimizu, R. Y.; Yokogawa, D.; Yanai, T. Multireference Perturbation Theory Combined with PCM and RISM Solvation Models: A Benchmark Study for Chemical Energetics. *J. Phys. Chem. A* **2021**, *125*, 8324–8336.

(60) Shiozaki, T.; Győrffy, W.; Celani, P.; Werner, H.-J. Communication: Extended Multi-State Complete Active Space Second-Order Perturbation Theory: Energy and Nuclear Gradients. *J. Chem. Phys.* **2011**, *135*, 081106.

(61) Battaglia, S.; Lindh, R. Extended Dynamically Weighted CASPT2: The Best of Two Worlds. *J. Chem. Theory Comput.* **2020**, *16*, 1555–1567.

(62) Battaglia, S.; Lindh, R. On the Role of Symmetry in XDW-CASPT2. *J. Chem. Phys.* **2021**, *154*, 034102.

(63) Nishimoto, Y.; Battaglia, S.; Lindh, R. Analytic First-Order Derivatives of (X)MS, XDW, and RMS Variants of the CASPT2 and RASPT2 Methods. *J. Chem. Theory Comput.* **2022**, *18*, 4269–4281.

(64) Nishimoto, Y. Analytic Gradients for Restricted Active Space Second-Order Perturbation Theory (RASPT2). *J. Chem. Phys.* **2021**, *154*, 194103.

(65) Nishimoto, Y. Analytic first-order derivatives of CASPT2 with IPEA shift. *J. Chem. Phys.* **2023**, *158*, 174112.

(66) You, Z.-Q.; Mewes, J.-M.; Dreuw, A.; Herbert, J. M. Comparison of the Marcus and Pekar partitions in the context of non-equilibrium, polarizable-continuum solvation models. *J. Chem. Phys.* **2015**, *143*, 204104.

(67) Aquilante, F.; Lindh, R.; Bondo Pedersen, T. Unbiased Auxiliary Basis Sets for Accurate Two-Electron Integral Approximations. *J. Chem. Phys.* **2007**, *127*, 114107.

(68) Aquilante, F.; Gagliardi, L.; Pedersen, T. B.; Lindh, R. Atomic Cholesky Decompositions: A Route to Unbiased Auxiliary Basis Sets for Density Fitting Approximation with Tunable Accuracy and Efficiency. *J. Chem. Phys.* **2009**, *130*, 154107.

(69) Ghigo, G.; Roos, B. O.; Malmqvist, P.-Å. A Modified Definition of the Zeroth-Order Hamiltonian in Multiconfigurational Perturbation Theory (CASPT2). *Chem. Phys. Lett.* **2004**, *396*, 142 – 149.

(70) Raggi, G.; Galván, I. F.; Ritterhoff, C. L.; Vacher, M.; Lindh, R. Restricted-Variance Molecular Geometry Optimization Based on Gradient-Enhanced Kriging. *J. Chem. Theory Comput.* **2020**, *16*, 3989–4001.

(71) Fdez. Galván, I.; Raggi, G.; Lindh, R. Restricted-Variance Constrained, Reaction Path, and Transition State Molecular Optimizations Using Gradient-Enhanced Kriging. *J. Chem. Theory Comput.* **2021**, *17*, 571–582.

(72) Fdez. Galván, I.; Lindh, R. Smooth Things Come in Threes: A Diabatic Surrogate Model for Conical Intersection Optimization. *J. Chem. Theory Comput.* **2023**, *19*, 3418–3427.

(73) Forsberg, N.; Malmqvist, P.-Å. Multiconfiguration Perturbation Theory with Imaginary Level Shift. *Chem. Phys. Lett.* **1997**, *274*, 196–204.

(74) Hehre, W. J.; Ditchfield, R.; Pople, J. A. Self-Consistent Molecular Orbital Methods. XII. Further Extensions of Gaussian-Type Basis Sets for Use in Molecular Orbital Studies of Organic Molecules. *J. Chem. Phys.* **1972**, *56*, 2257–2261.

(75) Hariharan, P. C.; Pople, J. A. The Influence of Polarization Functions on Molecular Orbital Hydrogenation Energies. *Theor. Chem. Acc.* **1973**, *28*, 213–222.

(76) Gozem, S.; Melaccio, F.; Valentini, A.; Filatov, M.; Huix-Rotllant, M.; Ferré, N.; Frutos, L. M.; Angeli, C.; Krylov, A. I.; Granovsky, A. A.; Lindh, R.; Olivucci, M. Shape of Multireference, Equation-of-Motion Coupled-Cluster, and Density Functional Theory Potential Energy Surfaces at a Conical Intersection. *J. Chem. Theory Comput.* **2014**, *10*, 3074–3084.

(77) Widmark, P.-O.; Malmqvist, P.-Å.; Roos, B. O. Density Matrix Averaged Atomic Natural Orbital (ANO) Basis Sets for Correlated Molecular Wave Functions. *Theoret. Chim. Acta* **1990**, *77*, 291–306.

(78) Roos, B. O.; Lindh, R.; Malmqvist, P.-Å.; Veryazov, V.; Widmark, P.-O. Main Group Atoms and Dimers Studied with a New Relativistic ANO Basis Set. *J. Phys. Chem. A* **2004**, *108*, 2851–2858.

(79) Dunning, T. H. Gaussian Basis Sets for Use in Correlated Molecular Calculations. I. The Atoms Boron through Neon and Hydrogen. *J. Chem. Phys.* **1989**, *90*, 1007–1023.

(80) Su, P.; Li, H. *J. Chem. Phys.* **2009**, *130*, 074109.

(81) York, D. M.; Karplus, M. A Smooth Solvation Potential Based on the Conductor-Like Screening Model. *J. Phys. Chem. A* **1999**, *103*, 11060–11079.

(82) Trueblood, K. N.; Goldish, E.; Donohue, J. A three-dimensional refinement of the crystal structure of 4-nitroaniline. *Acta Crystallogr.* **1961**, *14*, 1009–1017.

(83) Máximo-Canadas, M.; Modesto-Costa, L.; Borges Jr, I. Ab initio electronic absorption spectra of -nitroaniline in different solvents: Intramolecular charge transfer effects. *J. Comput. Chem. n/a*.

(84) Åke Malmqvist, P.; Roos, B. O. The CASSCF state interaction method. *Chem. Phys. Lett.* **1989**, *155*, 189–194.

(85) Millefiori, S.; Favini, G.; Millefiori, A.; Grasso, D. Electronic spectra and structure of nitroanilines. *Spectrochim. Acta* **1977**, *33A*, 21–27.

(86) Kovalenko, S.; Schanz, R.; Farztdinov, V.; Hennig, H.; Ernsting, N. Femtosecond relaxation of photoexcited para-nitroaniline: solvation, charge transfer, internal conversion and cooling. *Chem. Phys. Lett.* **2000**, *323*, 312–322.

(87) Farztdinov, V. M.; Schanz, R.; Kovalenko, S. A.; Ernsting, N. P. Relaxation of Optically Excited p-Nitroaniline: Semiempirical Quantum-Chemical Calculations Compared to Femtosecond Experimental Results. *J. Phys. Chem. A* **2000**, *104*, 11486–11496.

49

(88) Giovannini, T.; Cappelli, C. Continuum vs. atomistic approaches to computational spectroscopy of solvated systems. *Chem. Commun.* **2023**, *59*, 5644–5660.

(89) Sepali, C.; Goletto, L.; Lafiosca, P.; Rinaldi, M.; Giovannini, T.; Cappelli, C. Fully Polarizable Multiconfigurational Self-Consistent Field/Fluctuating Charges Approach. *J. Chem. Theory Comput.* **2024**, *20*, 9954–9967.

(90) Negishi, N.; Yokogawa, D. Lagrangian of extended multiconfigurational self-consistent field second-order quasidegenerate perturbation theory combined with reference interaction site model self-consistent field constraint spatial electron density. *J. Chem. Phys.* **2024**, *160*, 114104.

(91) Stålring, J.; Bernhardsson, A.; Lindh, R. Analytical Gradients of a State Average MCSCF State and a State Average Diagnostic. *Mol. Phys.* **2001**, *99*, 103–114.

(92) Bak, K. L.; Boatz, J.; Simons, J. First-Order Geometrical Response Equations for State-Averaged Multiconfigurational Self-Consistent Field (SA-MCSCF) Wave Functions. *Int. J. Quantum Chem.* **1991**, *40*, 361–378.

Graphical TOC Entry

CASPT2 + PCM